EurJOC
European Journal of Organic Chemistry

Review
doi.org/10.1002/ejoc.202200185

Chemistry Europe
European Chemical Societies Publishing

www.eurjoc.org

Homogeneous Systems Containing Earth-Abundant Metal Complexes for Photoactivated CO_2 Reduction: Recent Advances

Claudia Bizzarri*[a]

Photo-driven reduction of CO_2 into advantageous chemicals is a noteworthy pathway to close the carbon cycle and decrease carbon footprint. The use of visible light and ultimately solar radiation is extremely interesting in managing energy issues. Similarly, the employment of cost-effective materials guides to environmentally friendly applications. This Review addresses the homogeneous systems used for photoactivated the CO_2 reduction in the last years, highlighting the earth-abundant metal-based components. Besides those systems composed only of noble metal-free units, hybrid systems, also containing a noble metal-based complex, are also examined, revealing that research needs to increase the attention on more sustainable alternatives.

1. Introduction

In 2021, international summits and conferences on climate change were organized to discuss and take political action to oppose global warming. The outcome of the United Nations COP26 was a step forward, although small and disappointing in some perspectives.[1] Nevertheless, progress comes out from intensive scientific research. Scientists and, in particular, chemists have to bear responsibilities for the future and find a way to minimize negative human impacts on the environment. For many years, chemists have started to consider one of the major causes of the greenhouse effect, CO_2, not just as a combustion product but as a sustainable building block.[2] As nature converts carbon dioxide in biomass *via* photosynthetic processes, the exploitation of light as an energy source to activate CO_2 reduction is highly desirable. For this scope, researchers have developed in the last forty years an enormous number of homogeneous and heterogeneous systems that can absorb visible light and promote electron transfer, ending towards reduced products, which are essential intermediates in further chemical or industrial processes.[3] In those photocatalytic systems, we can distinguish three main components: a photosensitizer (PS), a catalyst (CAT), and a sacrificial electron donor (e-D). The PS absorbs a photon and is promoted to its excited state, which initiates the electron transfer. Depending on the redox potentials of PS in its excited state, it can go either a reductive quenching by the e-D or an oxidative quenching by the CAT. In the first process, the reduced PS will then transfer an electron to the catalyst, while in the second one, the oxidized PS is reduced back by the sacrificial electron donor (Scheme 1).

Typically, the electron donor is consumed during the reaction; thus, it is sacrificial. Although water would be the most environmentally friendly e-D, the water-splitting process might compete with the CO_2-reduction. Indeed, even in natural photosynthesis, separated compartments are responsible for water splitting and CO_2-reduction, which is then reduced by hydrogen equivalents NADPH. In the absence of spatially separated reactions, sacrificial electron donors are used. A vast choice is available, and the final selection depends on the redox properties and their reductant power.[4] Among the most used e-D in homogeneous photoactivated CO_2-reduction, there are amine derivatives. Triethylamine (TEA) and triethanolamine (TEOA) are employed in high amounts (up to 25% in volume). They are also used as a base in combination with other sacrificial electron donors. Nevertheless, a significant role in the capture of CO_2 by TEOA has been recently investigated, opening an alternative path.[5] Other widely used e-D are 1-

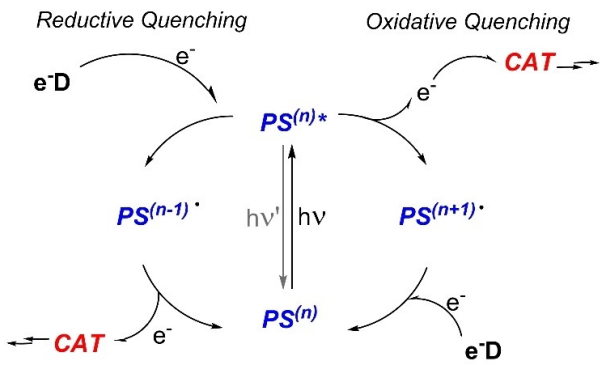

Scheme 1. General representation of the reductive (left) and oxidative (right) quenching processes and consecutive redox reactions.

[a] *Dr. C. Bizzarri*
Institute of Organic Chemistry,
Karlsruhe Institute of Technology,
Fritz-Haber-Weg 6, 76131 Karlsruhe, Germany
E-mail: bizzarri@kit.edu
https://www.ioc.kit.edu/bizzarri/english/index.php

benzyl-1,4-dihydronicotinamide (BNAH), a model for the natural NADPH, and 1,3-dimethyl-2-phenylbenzimidazoline (BIH), while sodium ascorbate (Asc^-) is the preferred e-D in water solutions (Figure 1).

As shown in Figure 2, the majority of the PS based on earth-abundant metals are heteroleptic copper(I) complexes.[6] Those complexes have attractive advantages, such as low cost, easy preparation, and high tunability. On the other end, the choice of solvent might influence their performance and stability since they populate a metal-to-ligand charge-transfer (MLCT) state upon excitation, which is sensitive to the polarity of the medium. Another drawback is the possible equilibrium with the relative homoleptic complex that is less performing. Nevertheless, those complexes are very promising, and their development has made a step forward. These heteroleptic Cu(I) complexes usually bear a commercially available diphosphine, *e.g.*, bis[(2-diphenylphosphino)phenyl] ether (DPEPhos) and 4,5-bis-(diphenylphosphino)-9,9-dimethylxanthen (Xantphos), and a tailor-made diimine, mostly based on phenanthroline. The bulky diphosphine has the role of stabilizing the Cu(I) complex from coordination with other species in solution, especially in its excited state, as it undergoes a Jahn-Teller distortion.[7] The diimine determines the final complex photophysical properties, as the lowest unoccupied molecular orbital (LUMO) is usually localized on the free π^* orbital of this ligand. For this reason, the Cu(I) complexes based on similar diimines present the maximum absorption of the ^{1}MLCT around the same value (see Table 1). This is also true comparing their redox properties in the ground state. Nevertheless, the different functional groups or sterically hindered substituents influence the radiative and non-radiative pathways of the excited state, leading to distinct emission and excited-state redox potentials.

Several organic chromophores have become desirable in photoredox catalysis[8] and employed as sustainable alternative photosensitizers in the photocatalytic reduction of CO_2 in more recent years.[9] These organic dyes are typically fluorescent, that is, their emissive excited-state is a singlet, which often prevents high efficiency of the photoinduced electron-transfer process, where long-lived excited states are beneficial. Thus, some strategies have been developed to increase spin-orbit coupling to enhance the population of the triplet excite-state. A possibility is the introduction of heavy atoms, inducing the "heavy-atom effect", as the case of the Eosin Y, that bears Br substituents, and the zinc-porphyrin covalently linked to the rhenium catalyst (see **Zn2** in Figure 2). Another method is the formation of donor-acceptor-dyads so that the charge transfer upon excitation and the following charge recombination causes the generation of a triplet state.

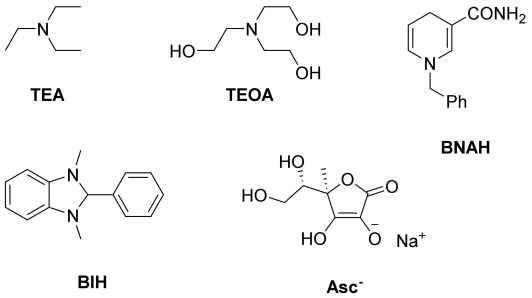

Figure 1. Chemical structures of the most common electron donors.

First-row transition metals, like Mn, Fe, Co, and Ni, have been used for new and efficient catalysts for CO_2 reduction. Their abundance in the earth's crust makes them appealing for future applications, having increased sustainability and a lower cost impact, among advantages. The fourth most abundant element in the earth's crust, with a concentration of 52157 ppm,[10] is iron, although the maximum percentage of this metal is found on the earth's core. For this reason, the design of efficient catalysts based on this metal is very attractive. Manganese's abundance is 774 ppm,[11] and cobalt and nickel are present in lower concentrations (26.6 ppm each).[12] Although this concentration is almost 30 times less than Mn and 1960 times less than Fe, they are still among earth-abundant metals, especially when compared with the abundance of noble metals. Nevertheless, it is critical to consider Co a sustainable metal. In fact, its presence is not homogeneously distributed on the earth's surface, but concentrated on specific zones, where increased supply risks are added to human rights violations.[13] This said, the study of newly developed Co-based catalysts can activate significant advances in understanding the mechanisms for CO_2-reduction.[14] On the other hand, the supply risks are considered lower in the case of nickel.[15] In nature, the active center of the carbon monoxide dehydrogenase (CODH) is a Fe–S cluster with a Ni nucleus, playing an essential role.[16] One of the first earth-abundant molecular systems for electrochemical CO_2 reduction was a Ni(II) complex.[17] As well, the first CO_2 reduction catalyst that presented outstanding efficiency in terms of turnover number (TON) and frequency (TOF) was also a Ni(II)-based N-heterocyclic-carbene complex.[18] Recently, discrete molecular nickel

Claudia Bizzarri received her B.Sc. and M.Sc. in Chemistry at the University of Rome "Tor Vergata" (Italy). In 2011 she obtained her Ph.D. working on luminescent Ir(III) and Cu(I) complexes for optoelectronic applications at the University of Münster (Germany). She was a visiting research student at the University of Minnesota Duluth (USA) in 2007 and at the University College London (UK) in 2010. After a couple of years as a Process Engineer at AIXTRON SE (Aachen, Germany), she was a post-doc at the CAT Catalytic Center of the University RWTH Aachen. Since the end of 2016, Claudia Bizzarri is an independent Junior Group Leader at the Karlsruhe Institute of Technology (KIT), and in 2020 she was appointed as Lecturer and as KIT Associate Fellow. Her research interests focus on photoactive compounds based on earth-abundant metals. Her coordination metal complexes find applications in visible-light driven photochemistry (especially for CO_2 reduction) and bioimaging.

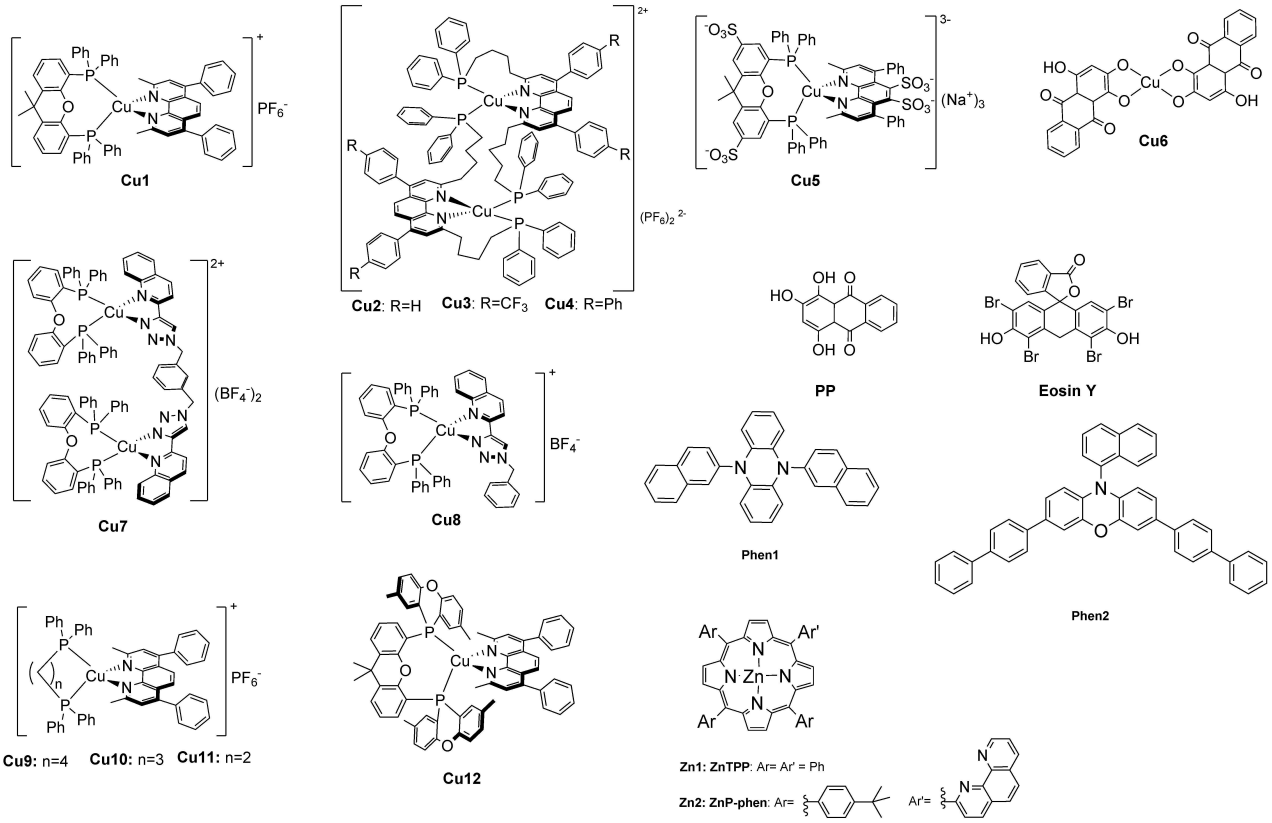

Figure 2. Chemical structures of the earth-abundant metal-based complexes and organic molecules used as photosensitizers presented in this review.

Table 1. Selected photophysical and electrochemical properties of photosensitizers (PS) discussed in this review.[a]

PS	λ_{exc} /nm	λ_{em} /nm	E_{ox} /V[b]	E_{red}/V [b]	E_{ox}*/V [b]	E_{red}*/V [b]	Ref.
Cu1	389[c]	569[c]	0.93	−2.05	−1.75	0.63	[42, 73]
Cu2	379	624	0.89[d]	−1.95[d]	−1.10[d]	0.04	[34]
Cu3	386	654	–	−1.83[d]	–	–	[33]
Cu4	381	630	–	−1.91[d]	–	–	[33]
Cu5[e]	387	565	1.01[f]	−1.72[f]	−1.61[f]	0.90[f]	[37]
Cu6[g]	566	693	–	−1.05,[f] −1.50,[f] −1.69[f]	−1.61[f]	0.37[f]	[35]
Cu7	388	650	1.00	−1.95	−1.31	0.75	[39]
Cu8	398	640	0.95	−2.09	−1.75	0.6	[39]
Cu9	387	605	–	−1.96[d, h]	–	–	[41]
Cu10	400	608	–	−1.95[d, h]	–	–	[41]
Cu11	411	608	–	−1.93[d, h]	–	–	[41]
Cu12[i]	398	536	0.83	−2.10	−1.84	0.57	[29b]
Zn1	549[j]	646[j]	0.42[i]	−1.79[i]	–	–	[74]
Zn2[k]	450	615	0.30	−1.79	–	–	[43]
PP	506, 540	561, 599	–	−0.66 [f]	–	–	[27, 75]
4CzIPN	539		1.11	−1.62	−1.17	0.66	[76]
Eosin Y	556		0.37	−1.47	−1.82	0.72	[76]
Phen1[k]	343	654	0.21[f]	–	−1.69[f]	–	[28, 77]
Phen2[k]	388	506	0.65[f]	–	−1.80[f]	–	[28, 77]
$Ru(bpy)_3$ $(PF_6)_2$	452	615	1.29[f]	−1.33[f]	−0.81[f]	0.77[f]	[78]
$Ru(phen)_3$ $(PF_6)_2$	422	610	1.26[f]	−1.36[f]	−0.87[f]	0.82[f]	[78]
***fac*-$Ir(ppy)_3$**	375	494	0.77[f]	−2.19[f]	−1.73[f]	0.31[f]	[78]
$Ir(dFppy)_3$	378	476	0.94[f]	−1.87[f]	−1.28[f]	0.36[f]	[79]
$Ir(ppy)_2(qpy)$ PF_6	420	–	0.96	−1.37	−1.47	1.06	[53]

[a] Data are in MeCN unless otherwise noted. [b] E versus Fc/Fc^+. [c] in THF. [d] E versus $Ag/Ag/NO_3$. [e] in saturated aqueous $NaHCO_3$ solution 0.1 M (pH 6.7). [f] E versus SCE. [g] in DMF. [h] in DMA/TEOA (4 : 1). [i] in Toluene. [j] in CH_2Cl_2. [k] in DMA.

catalysts used in photocatalytic CO_2 reduction have been reviewed, focusing on their reactivity and selectivity.[19] In general, homogeneous molecular catalysts based on 3d-transition metals can convert CO_2 to two-electrons reduction products, CO and $HCO_2(H)$. Rarely methane or methanol have been observed in photoactivated CO_2-reduction by means of these molecular catalysts. This is the case because the metallic nuclei undergo discrete electron transfer processes, while on the surface of semiconductors, multiple electrons are available in one step. Electrochemical measurements, like cyclic voltammetry, are very useful for mechanistic studies when performed in the same solvent (and cosolvent) of the photocatalytic experiments. In this manner, the thermodynamics of the electron transfer processes can be determined. Furthermore, under CO_2 atmosphere, a catalytic current can be observed, and the oxidation state of the metal, at which CO_2 is adsorbed and starts to be reduced, is established. However, caution should be paid when comparing redox potentials of different CO_2-reduction catalysts, since solvent effects cannot be under-evaluated.[20]

Further mechanistic insights are often given by density-functional theory (DFT), which also helps in understanding the most plausible coordination mode of CO_2 with the metal center of the catalyst (Figure 3).[21]

Many comprehensive reviews are present in the literature, focusing on different aspects of the CO_2-reduction catalysts.[22] Herein, the focus will be given to advances in this field in the last five years (2017–2021), as this research area is rapidly evolving, and many new stimulating results have been achieved. In particular, an overview of the latest homogeneous photocatalytic systems for CO_2 reduction will be presented that make use of earth-abundant metal complexes or organic molecules.

2. Noble-Metal-Free Molecular Photocatalytic Systems

Photoactivated CO_2-reduction systems that use only earth-abundant elements are still a minority. Nevertheless, a significant increase in such works can be observed in the last five years. The most noticeable results of every cited work are summed up in Table 2 together with the reaction conditions.

Manganese can exist in six different oxidation states. CO_2-reduction catalysts based on Mn(I) are usually carbonyl complexes (see Figure 4). The structures of those catalysts resemble those of the rare-metal Re(I), which belong to the

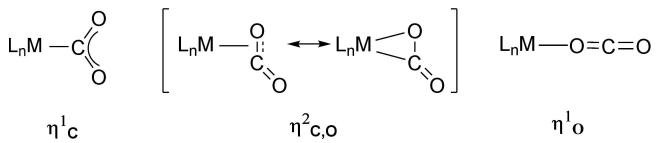

Figure 3. Structural CO_2-Metal patterns.

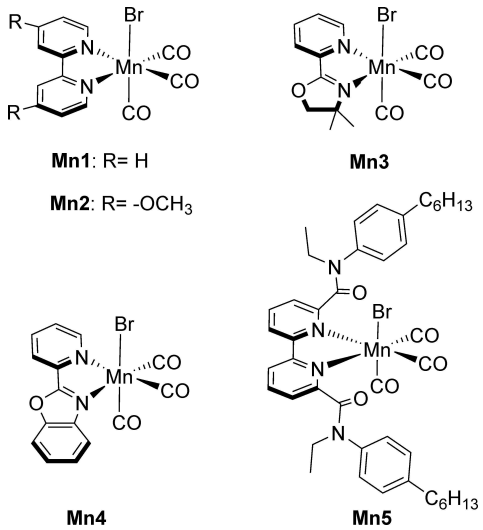

Figure 4. Chemical structures of the Mn(I) carbonyl complexes that are discussed in this review.

same group, yet the efficiency shows that improvements are necessary.

Different substituents on the bipyridine ligand in complexes **Mn1-3** influence not only their electrochemical properties, but also the selectivity of the CO_2 reduction products.[23] In fact, when using a dinuclear Cu(I) complex as a photosensitizer, **Cu2**, under irradiation at 436 nm for 2 hours, **Mn1** produces formic acid HCO_2H as the primary product with a TON of 157 and a quantum yield Φ of 30%, and with a selectivity of 74.6% (Table 2, Entry 1). When **Mn2** is used, the selectivity drops to 28.5%, and the primary product is CO (TON 164, Φ 33%). The photocatalytic system consisting of **Cu2** and **Mn2** was tested further and showed that at longer irradiation time (24 h) the system is photostable, and also the product distribution increases in favor of carbon monoxide (Table 2, entry 2). Ishitani and coworkers claim that the suspension of the catalysis after 24 h is due to the consumption of the electron donor BIH. The catalyst with a mesityl substituent in position 6, **Mn3**, produces CO with the highest selectivity (TON_{CO} 208; TON_{HCO2H} 5; Selct.CO: 96.6%) even after only 2 hours of irradiation. Those systems also produced molecular hydrogen, although in tiny amounts ($TON_{H2} < 4$). The proposed reaction mechanism indicates a reductive quenching of the **Cu2*** by BIH. The reduction potential of **Cu2** was observed in *N,N*-dimetilacetamide (DMA) at −1.92 V (vs $Ag/AgNO_3$). Also, the oxidized benzoimidazole, in its deprotonated form $BI^{\bullet}$, can reduce the **Cu2** to **Cu2**$^{\bullet-}$. Thermodynamically, reducing the Mn catalysts by this **Cu2**$^{\bullet-}$ species is feasible, and a de-halogenated 17-electron Mn complex is produced, consequently dimerizing to Mn–Mn species. By a further electron transfer process, the negative mononuclear species $Mn(bpy)(CO)_3^-$ can be formed. In the case of **Mn3**, this 5-coordinate 18-electron species reacts with CO_2, while **Mn1** and **Mn2** react with CO_2 in their dimeric forms. The total quantum efficiency of the reduction of CO_2 is up to 57% for **Mn3**, considering the sum of the reduced products of CO_2.

Table 2. Photocatalytic CO_2-reduction using noble-metal-free molecular systems.

Entry	PS	CAT	e-D	Solvent	λ_{exc}	Irradiation time	Products	TON	Selectivity [%]	Φ [%]	Ref.
1	**Cu2** (0.25 mM)	**Mn1** (0.05 mM)	BIH (10 mM)	DMA/TEOA (4:1)	436 nm	2 h	HCO_2H CO H_2	157 50 4	74.6 23 1.7	30 2 –	[23]
2	**Cu2** (0.25 mM)	**Mn2** (0.05 mM)	BIH (0.1 M)	DMA/TEOA (4:1)	436 nm	24 h	CO HCO_2H H_2	1004 310 68	72.6 22.4 5	33 24 –	[23]
3	**Cu2** (0.25 mM)	**Mn3** (0.05 mM)	BIH (0.1 M)	DMA/TEOA (4:1)	436 nm	2 h	CO HCO_2H H_2	208 5 0.5	97.4 2.4 0.2	41 0.03 –	[23]
4	**Cu1** (1 μM)	**Mn4** (0.01 μM)	BIH (0.1 M)	MeCN/TEOA (5:1)	>415 nm	5 h	CO	1058	>99	0.47	[24]
5	**Cu1** (1 μM)	**Mn5** (0.01 μM)	BIH (0.1 M)	MeCN/TEOA (5:1)	>415 nm	5 h	CO	113	>99	–	[24]
6	**Zn1** (1.9 μM)	**Mn6** (1.5 μM)	TEA (5 ml)	MeCN/H_2O (95:5)	625 nm	40 min	CO	0.30	–	–	[25]
7	**PP** (0.2 mM)	**Fe1** (2 μM)	TEA (50 mM)	MeCN/H_2O (1:9) + $NaHCO_3$ (0.1 M)	>420 nm	47 h	CO H_2	60 3	95 5	–	[27]
8	**Phen1** (1 mM)	**Fe1** (10 μM)	TEA (0.1 M)	DMF + TFE (0.1 M)	436 nm	102 h	CO H_2	60 6	90 10	–	[28]
9	**Phen2** (1 mM)	**Fe1** (10 μM)	TEA (0.1 M)	DMF + TFE (0.1 M)	436 nm	102 h	CO H_2 CH_4	140 23 29	72.9 12 15.1	0.47 (for CH_4 in CO atm)	[28]
10	**Cu1** (5 μM)	**Fe2** (1 μM)	BIH (0.1 M)	NMP/TEOA (5:1)	400-700 nm	5 h	CO H_2	487 7	99 1	13.3	[29a]
11	**Cu1** (0.8 mM)	**Fe2** (0.16 mM)	BIH (150 mg)	Bmpyrr $(N(CN)_2)$: TEOA (4:1)	400-700 nm	5 h	CO H_2	79 ≤3	>92 ≤8	–	[29b]
12	**Cu12** (5 μM)	**Fe2**	BIH (150 mg)	NMP/TEOA (5:1)	400-700 nm	5 h	CO H_2	505 23	93 7	–	[29b]
13	**Cu1** (0.5 mM)	**Fe3** (0.025 mM)	BIH (50 mM)	DMF/TEOA (4:1)	>400 nm	8 h	CO H_2, HCO_2^-	260 (37 μmol) (1.8 μmol)	63	1.6 (1 h)	[30]
14	**PP** (0.05 mM)	**Fe4** (0.05 mM)	BIH (0.1 M)	DMF + TFE (5%)	460 nm	15 h	CO H_2	544 4	99.3 0.7	0.12% (3 h)	[31]
15	**4CzIPN** (50 μM)	**Fe5** (10 μM)	TEA (0.28 M)	DMF/H_2O (3:2)	420-650 nm	3 h	CO H_2	2250 16	99.3 0.7	2.04	[32a]
16	**4CzIPN** (100 μM)	**Fe6** (10 μM)	TEA (0.28 M)	DMF/H_2O (3:2)	420-600 nm	2 h	CO H_2	6320 35	99.4 0.6	9.5	[32b]
17	**4CzIPN** (50 μM)	**Fe7** (4 μM)	TEA (0.28 M)	DMF/H_2O (3:2)	440 nm	2 h	CO H_2	14956 55	99.6 0.4	2.8	[32c]
18	**Cu2** (0.025 mM)	**Fe8** (0.05 mM)	BIH (50 mM)	MeCN/TEOA (5:1)	436 nm	24 h	CO H_2	362 111	76.5 23.5	7.1	[33]
19	**Cu3** (0.025 mM)	**Fe8** (0.05 mM)	BIH (50 mM)	MeCN/TEOA (5:1)	436 nm	24 h	CO H_2	440 186	70.3 29.7	14.1	[33]
20	**Cu4** (0.025 mM)	**Fe8** (0.05 mM)	BIH (50 mM)	MeCN/TEOA (5:1)	436	24 h	CO H_2	445 141	75.9 24.1	5.3	[33]
21	**Cu6** (0.1 mM)	**Fe9** (0.2 μM)	BIH (100 mM)	DMF	White light	23 h	CO H_2	16109 843	95 5	6.0	[35]

Table 2. continued

Entry	PS	CAT	e-D	Solvent	λ_{exc}	Irradiation time	Products	TON	Selectivity [%]	Φ [%]	Ref.
22	**Cu1** (0.05 mM)	**Co1** (0.05 mM)	TEA (5% vol)	DMF	> 400 nm	24 h	CO	13	–	–	[36]
23	**Cu5** (0.5 mM)	**Co3** (5 μM)	Ascorbate (0.1 M)	0.1 M $NaHCO_3$ buffer (pH: 6.7)	> 400 nm	4 h	CO H_2	2680 820	77 23	1.62	[37]
24	**Cu5** (0.5 mM)	**Co5** (5 μM)	Ascorbate (0.1 M)	0.1 M $NaHCO_3$ buffer (pH: 6.7)	> 400 nm	4 h	CO H_2	1085 127	90 10	–	[37]
25	**Cu5** (0.5 mM)	**Co4** (5 μM)	Ascorbate (0.1 M)	0.1 M $NaHCO_3$ buffer (pH: 6.7)	> 400 nm	12 h	CO H_2	4000 460	90 10	5.7	[38]
26	**Cu5** (0.5 mM)	**Co6** (5 μM)	Ascorbate (0.1 M)	0.1 M $NaHCO_3$ buffer (pH: 6.7)	> 400 nm	8 h	CO H_2	460 140	77 23	–	[38]
27	**Cu7** (0.5 mM)	**Ni1** (0.1 mM)	BIH (20 mM)	MeCN/TEOA (5 : 1)	420 nm	4 h	CO	8.1	> 99	2.1	[39]
28	**Cu8** (1 mM)	**Ni1** (0.1 mM)	BIH (20 mM)	MeCN/TEOA (5 : 1)	420 nm	4 h	CO	4.3	> 99	1.0	[39]
29	**EosinY** (2 mM)	**Ni2** (4 μM)	TEOA (0.4 mM)	EtOH/H_2O (1 : 1)	420 nm	10 h	HCO_2^-	14000	> 99	4.1	[40]

In the groups of Beller and Francke, Mn(I)-carbonyl complexes were developed using as a chelating diimine a pyridine-oxazole (**Mn4**) or pyridine-benzoxazole (**Mn5**).[24] These complexes were able to selectively reduce carbon dioxide to CO (Table 2, Entries 4 and 5). The catalysis was photoactivated by **Cu1**, which was generated *in situ*. Also in this case, a reductive quenching of the excited PS by BIH is the first electron transfer of the photocatalytic cycle. The dehalogenative reduction of the Mn(I) catalyst follows, and although the radical species is in equilibrium with the dimer Mn–Mn, the proposed mechanism shows that the catalytic form is the mononuclear radical. The most efficient catalyst was **Mn4**, which gave a TON of 1058. The quantum yield of this photocatalytic system was calculated to be 0.47 %.

Weinstein group chose a bipyridine with sterically hindering substituents to develop a new Mn(I)-carbonyl catalyst (**Mn6**, Figure 4), preventing the dimerization of its reduced species.[25] This complex shows electrocatalytic activity in respect to CO_2 in a solution of MeCN with 5 % water, and the turnover frequency at the potential required for the maximum rate was higher than the corresponding Re(I) carbonyl complex. However, photocatalysis was not efficient. In combination with the tetraphenylporphyrin **Zn1** as PS, under 625 nm irradiation, the production of CO had a TON of only 0.3 (Table 2, Entry 6). Among possible optimization strategies, an essential role could be played by the addition of triethanolamine (TEOA), which acts not only as a base, but its presence can enhance the CO_2 capturing abilities of Mn(I) complexes, as proven by recent studies.[26]

Among the first catalysts used in CO_2-reduction are iron porphyrins, and those have been continuously developed further for this aim. In 2017, the groups of Robert and Bonin presented a photocatalytic system based on Fe(III)-tetra(*N,N,N*-trimethylaniline)porphyrin (**Fe1** in Figure 5), in combination with purpurin (**PP**) as an organic photosensitizer, under white light irradiation ($\lambda > 420$ nm).[27] Interestingly, the photocatalysis was performed in an aqueous solution (MeCN/H_2O, 1 : 9), yielding a high selectivity of CO (95 %), and only a small amount of molecular hydrogen was formed (Table 2, entry 7). The purpurin absorbs visible light with a maximum at 477 nm in this solvent mixture, and it is reductively quenched by triethylamine (TEA). An oxidative quenching by **Fe1** is not happening, although thermodynamically feasible. The reduced $\mathbf{PP}^{2-}$ species can reduce Fe(III) to Fe(II), but not further. Thus, a more potent reductant was postulated to form upon excitation of the $\mathbf{PP}^{2-}$ species, which is quenched further by TEA, making the reduced species $\mathbf{PP}^{3-}$, able to reduce Fe(II) to Fe(I) and to Fe(0). These last reductions are thermodynamically feasible, if significant work terms are taken into consideration in the calculation of the free energy ΔG, assuming they are purely electrostatic. CO_2 binds the catalyst in its Fe(0) species and this adduct is stabilized thanks to the positive charge on the aniline substituents. One year later, the groups of Robert and Lau reported a photocatalytic system using the same iron-porphyrin **Fe1**.[28] In this case, phenoxazine derivatives were used as PS (**Phen1** and **Phen2**, Figure 2), and TEA (0.1 M) as e-D. The catalytic components were dissolved in a *N,N*-dimeth-

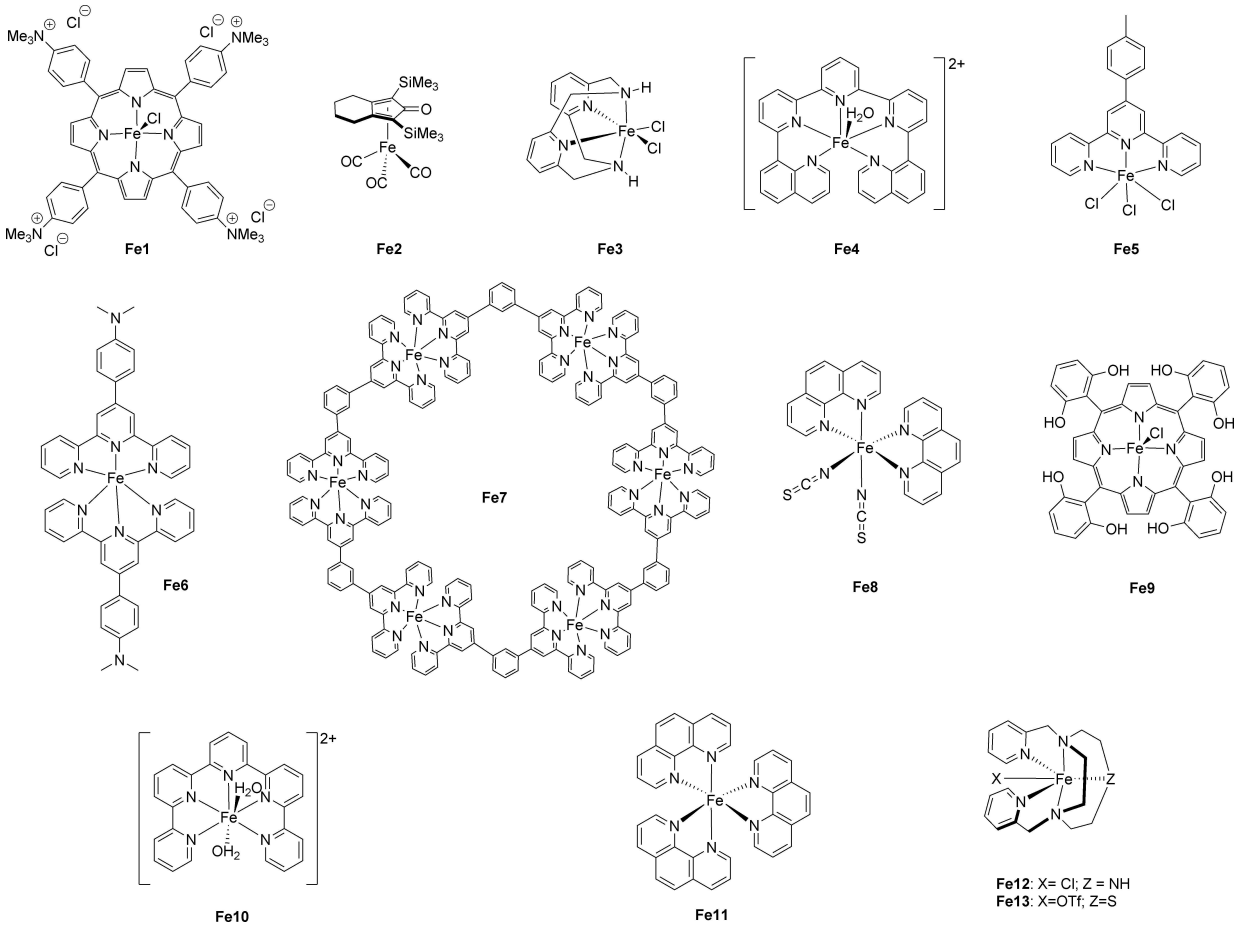

Figure 5. Iron-based catalysts discussed in this review.

ylformamide (DMF) solution with 0.1 M trifluoroethanol (TFE) as a proton donor. Irradiation with blue light (436 nm) generates the excited state of **Phen1**/**Phen2**, oxidatively quenched by the catalyst **Fe1**. The reactions yielded CO as a major product, with TONs up to 140 after four days (Table 2, entries 8 and 9). Surprisingly, when **Phen2** was used, an additional reduction product of CO_2 was detected: methane (TON_{CH4} 29). This led to further investigations, repeating the photocatalysis under an atmosphere of solely CO. In fact, carbon monoxide is an intermediate, and a TON_{CH4} of 80 with a quantum yield of 0.47% was reached after 102 hours of irradiation. The long reaction times demonstrate also the high photostability of **Phen2** and **Fe1**.

The iron cyclopentadienone complex **Fe2** was used in the investigation led by Beller and coworkers, combined with the *in situ* generated Cu(I) complex **Cu1**.[29] In the first work, the catalytic components were dissolved in a mixture of *N*-methyl-2-pyrrolidone (NMP) and TEOA,[29a] while in the following paper, the photoactivated CO_2-reduction was evaluated in different classes of ionic liquids (ILs).[29b] In both cases, the sacrificial electron donor BIH was used, proving that the photosensitizer **Cu1*** excited state was reductively quenched. The **Cu1**$^-$ then reduces the iron-cyclopentadienone. Subsequent reduction of CO_2 yields CO in high selectivity (up to 99%). In the case of the organic solvent mixtures, under white light irradiation for 5 hours, the turnover number of CO was 487, and the quantum efficiency of the reaction was 13.3%, measured after 2 hours (Table 2, entry 10). The selectivity of CO versus molecular hydrogen was decreased to 93%, when using **Cu12** as photosensitizer (Table 2, entry12).[29b] The use of ionic liquids as a solvent for the photoactivated CO_2 reduction has some advantages since they are not volatile (and therefore, more sustainable in respect to common organic solvents), and they can facilitate CO_2 capture. The most suitable IL for CO_2 reduction purposes was found to be 1-butyl-1-methylpyrrolidinium dicyanamide ([Bmpyrr] [$N(CN)_2$]). Because of the higher viscosity, the photosensitizer was added already as **Cu1** and not formed *in situ* as in previous cases. The TON_{CO} was 79 after 5 hours and the selectivity of 92% (see Table 2, entry 11). A pyridinophane Fe(II) catalyst, **Fe3**, was prepared and investigated by Sakai and coworkers.[30] The tetraazacyclododecane ligand forces the Fe(II)Cl_2 core in a strained geometry (see Figure 5). However, when it crystallizes, it forms a Fe(III) dimer with a μ-oxo-bridge. In the same work, corresponding complexes based on Co(II), Ni(II) and Zn(II) were also prepared, but their catalytic performances were much lower in comparison to those of the **Fe3**. The best photocatalytic conditions were found to be in DMF/TEOA mixture, using **Cu1** as PS and BIH as e-D.

After 8 hours of visible light irradiation, CO was the main product (TON_{CO} 260) (Table 2, entry 13). The lability of the complex **Cu1**, forming the not efficient homoleptic diimine complex, was demonstrated to be an issue for the efficiency of photocatalysis. In fact, when the chelating phosphine was added further (2 equiv. in respect to the **Cu1** complex), the TON_{CO} and the selectivity increased to 565 and 84%, respectively. The quantum efficiency was evaluated 1.6% after 1 hour of irradiation.

Fe4 is an iron(II) complex coordinated to a pentadentate bis(quinoline)-terpyridine ligand. The sixth coordinative bond of Fe(II) is occupied by a solvent molecule, such as water or MeCN.[31] In DMF, this catalyst presents three reduction potentials: the first one (-0.80 V *vs.* SCE) is attributed to redox couple Fe(II)/Fe(I), the second one refers to Fe(I)/ Fe(0), and it appears at −1.06 V; while the third one is at lower potentials and is attributed to ligand reduction (−1.78 V). A catalytic current was observed with the onset at −1.5 V when the electrochemical measurement was performed under CO_2 atmosphere. Thus, photocatalysis was tested, dissolving the same equivalents of **Fe4** and **PP** in DMF and irradiating the solution at 460 nm for 15 hours. The turnover number of the carbon monoxide produced was 544, with a selectivity of 99.3% in respect to H_2 (Table 2, entry 14). Traces of formate were found in the liquid phase analysis. The catalysis starts with the reductive quenching of **PP*** by the e-D BIH and continues until the catalyst is not deactivated. The authors suggested that 5% of TFE was necessary to help the cleavage of the bond between the metal core and the produced CO. An analogous compound based on Ni(II) was tested in the same conditions and gave poorer results (TON_{CO} 15).

The organic compound 2,4,5,6-Tetrakis(9*H*-carbazol-9-yl) isophthalonitrile (**4CzIPN**), known as thermally-activated delayed fluorescence (TADF) emitter, was used as photosensitizer in the photoactivated CO_2-reduction together with three iron-based catalysts, **Fe5**, **Fe6**, and **Fe7**, by Chao and collaborators. In particular, the similarity of the ligands used for coordinating the metal core, allows us to compare the activities of these complexes in a systematic manner.[32] The homogeneous photocatalysis was conducted in a mixture of DMF/H_2O (3:2) with TEA (0.28 M) as sacrificial e-D. In all cases, **4CzIPN** was reductively quenched by TEA, and its reduced form reduces the iron catalyst in turn. The heteroleptic **Fe5** presents the coordination of iron to three chlorine atoms. Thus, it is in oxidation state +3, while the homoleptic **Fe6** presents Fe(II).This is also confirmed by cyclovoltammetry as the **Fe5** shows an additional redox process in the positive potentials, attributed to the reduction of Fe(III) to Fe(II).[32a] The role of water in the solvent mixture was postulated to facilitate the reduction of the Fe, and the catalytic potential under CO_2 atmosphere was indeed positively shifted in respect to that found in only DMF. When no water was used, **Fe5** produced CO with a TON of 133 after 3 hours, while in the DMF/H_2O mixture, TON_{CO} reached 2250. The quantum yield of the reaction was 2.04% (Table 2, entry 15). The homoleptic complex **Fe6** gave almost three times more efficient results in the same conditions since TON_{CO} was 6320 with 9.5% quantum yield (Table 2, entry16).[32b] This increased efficiency can be attributed to the different substituents on the terpyridine. In **Fe6**, the ligand has the electron-donating group -$N(CH_3)_2$ in *para* to the phenyl substituent of the central pyridine. The authors speculate that this is sufficient to enhance the nucleophilicity of the iron center and therefore facilitates the adduct formation with CO_2. The metallo-supramolecular assembly **Fe7** contains six Fe(II) centers.[32c] The photocatalysis using **Fe7** gave the best selectivity to CO (99.6%), among the catalysts **Fe5**, **Fe6** and **Fe7**, and an increased TON_{CO} (14956) (Table 2, entry 17). The authors claim that the terpyridin ligand might act as an e- reservoir and they are reduced by **4CzIPN** in its reduced state. However, the increased efficiency of **Fe7** might also be due to the presence of additional 5 equivalents of Fe(II) in respect to **Fe5** and **Fe6**.

Binuclear Cu(I) complexes **Cu2**, **Cu3**, and **Cu4** (see Figure 2) were prepared and employed as photosensitizers by Takeda *et al.* The photocatalytic system consisted of a MeCN/TEOA solution (5:1) where the Cu(I) PS was dissolved together with the iron-based catalyst **Fe8**, using BIH as electron donor, which initiates a reductive quenching.[33] The three photocatalytic systems gave comparable results, producing CO as the major component and a minor amount of H_2 (Table 2, entries 18, 19, and 20). The same iron complex was used previously by the group of Ishitani, also in combination with the PS **Cu2**. However, the TONs of the produced CO were smaller (TON 95).[34] Most probably, the reason why the photocatalysis in the more recent work gave higher TON is related to the lower concentration of the catalysts used. After 24 hours of irradiation, the **Cu3** and **Fe8** gave the highest TON of 445, with a selectivity of CO up to 75.9% (Table 2, entry 20). Nevertheless, the highest quantum yield was obtained when using **Cu3** (14.1%). The substituents on the phenyl rings of the bathocuproine are responsible for the distinct redox properties of the Cu(I) complexes, therefore the different oxidation power of the three binuclear complexes in their excited state, influencing the quantum yield of the photochemical reaction.

In the work of Han's group, a redox-active Cu(II) metal is coordinated to two purpurine moieties (**Cu6** in Figure 2) and is used as efficient PS in combination with the iron-porphyrin **Fe9**.[35] Thanks to the two equivalents of the ligand, **Cu6** shows a more intense absorption in respect to the one of **PP** alone. This band is bathochromic shifted, probably due to the interaction of the dianion hydroxyanthraquinone with Cu(II). The complex **Cu6** showed also catalytic activity versus CO_2, but the best results were obtained when it was used in a DMF solution with **Fe9** as catalyst and BIH as sacrificial e-D. In particular, under white light irradiation for 23 hours, carbon monoxide was produced with a TON of 16109 and a selectivity of 95% in respect to H_2. Traces amounts of formic acid were also detected. The quantum efficiency was 6.0% in the first hour of the reaction. According to the mechanism suggested by the authors, BIH can reduce **Cu6**, and four molecules of CO_2 can be covalently bounded to the PP^-ligands. This *in situ*-formed complex is the effective photosensitizer, which is reductively quenched by another molecule of BIH and then can either reduce CO_2 to CO (but slowly) or reduce the iron-porphyrin **Fe9**, which then continues the cycle with carbon dioxide.

In the latest work of the group of Schwalbe, a cobalt complex was prepared with the macrocyclic ligand 1,4-di-(picolyl)-1,4,7-triazacyclononane, (**Co1**, Figure 6).[36] The same ligand was used also for the coordination with Fe(II) and Ni(II), and the photoactivated CO_2-reduction was mainly tested in combination with an iridium photosensitizer (*vide infra*). As **Co1** gave the highest efficiency in that system, it was tested also in combination with the photosensitizer **Cu1** (Table 2, entry 22). However, the production of CO dropped to 13 as the turnover number, after 24 hours of irradiation. The lower performance upon long irradiation time was attributed to a fast decomposition of the **Cu1** photosensitizer, although kinetic studies revealed that in the first two hours of irradiation, the noble-metal-free catalytic system shows higher conversion, while the system with Ir(III)-PS presents an induction period.

A fully aqueous media (*i.e.* $NaHCO_3$ buffer) was used for the photochemical CO_2-reduction using the water-soluble PS **Cu5** and the porphyrin-based Co catalysts **Co3**, **Co4**, **Co5** and **Co6**, and sodium ascorbate as e-D.[37,38] In all *meso*-positions of the macrocycle, the aromatic ring of the first two porphyrins are *N*-methyl-pyridinium substituent (in *para* for **Co3** and in *ortho* for **Co4**), **Co5** has a phenyl-sulfonate, and **Co6** has a trimethylaminophenyl (see Figure 6). For four hours, the CO_2-saturated reaction mixtures were irradiated with white light (> 400 nm). Catalyst **Co3** converted more than the double amount of CO_2 into CO, in respect to **Co5** (TON(**Co3**): 2680; TON(**Co5**): 1085). Nevertheless, the parallel production of H_2 was increased, lowering the selectivity towards CO to 77% (Table 2, entries 23 and 24). The maximum rate of the photocatalysis was found to be at 5 μM catalyst concentration, avoiding that the Soret band of the porphyrin works as an inner filter, since it overlaps with the MLCT absorption of **Cu5**. The production of CO stopped after 4 h because of the degradation of the PS. Thus, upon addition of fresh PS the photocatalysis was repristinated. The authors postulate that the multielectron reductions are necessary before the reduction of CO_2 can be activated, because of the *N*-methylpyridinium moieties, which act as e- acceptors. These events are thermodynamically favored by **Cu5**$^{\bullet-}$. An oxidative quenching of Cu* by **Co3** is also possible because of the cathodic values of **Cu5***, which are similar to the reduction potential in the ground state (see Table 1). Nevertheless, the major pathway is the reductive quenching by ascorbate.

A couple of years later, the same group improved the efficiency of the photoactivated CO_2 reduction with catalyst **Co4**, reaching 4000 of TON_{CO} and a selectivity of 90% (Table 2, entry 25).[38] Here, the four N-methylated pyridines are attached in *ortho* to the macrocycle. The reduction potentials of **Co4** are cathodically shifted compared to those for **Co3**, maybe because of the enhanced steric hindrance, avoiding the coplanarity of the pyridinium and the porphyrin. This fact promotes the

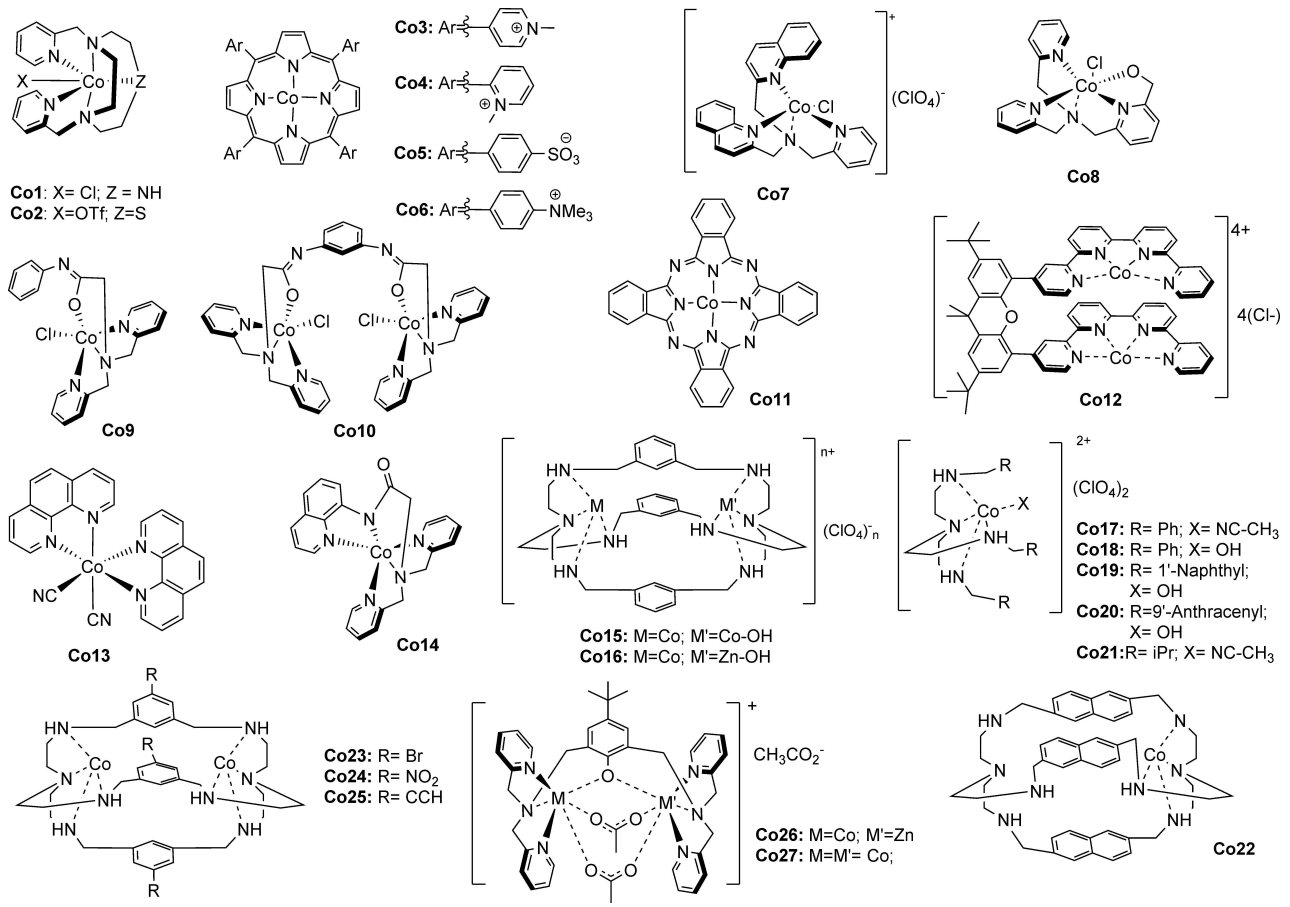

Figure 6. Co(II)-based catalysts discussed in this review.

catalytic process. Indeed, the cathodic onset measured electrochemically under CO_2 atmosphere occurs after the second reduction of **Co4**, indicating that the 2 e- reduced species of this catalyst promotes CO_2 activation, which is much favored in respect to the 4 e- or 5 e- species of **Co3**. Other newly developed Co-based catalysts were used in combination with noble-metal-based PS, therefore they are reported in the pertinent paragraph (*vide infra*).

In the last five years, many articles reported new efficient photocatalytic systems using Ni(II)-based complexes as CO_2-reduction catalysts. However, only a minority employed them in a fully noble-metal-free system, as reviewed here below.

The complex obtained coordinating Ni(II) with 1,4,8,11-tetraazacyclotetradecane (cyclam), **Ni1** (Figure 7), has been known to be active towards CO_2-reduction for almost forty years.[17] In 2020, it was combined with molecular photosensitizers based on Cu(I), achieving the first earth-abundant homogeneous photocatalytic system employing **Ni1**.[39] The photosensitizer **Cu7** is the binuclear complex of **Cu8**, and they are both stable in acetonitrile solutions for weeks. Photocatalytic experiments were conducted in a mixture 5:1 of MeCN/TEOA, and BIH was used as electron donor, which reductively quenches Cu*. After four hours of irradiation at 420 nm, **Ni1** produced carbon monoxide only, with a TON of 8.1, when **Cu7** was the PS, and with a TON of 4.3, when **Cu8** was used (Table 2, entries 27 and 28). Although the amount of produced CO was low, the quantum yield of the reactions was comparable to other more efficient catalytic systems, reaching 2.1% with **Cu7**, suggesting that further optimization of the catalyst concentration could increase also the TON values.

A neutral Ni(II) complex, **Ni2**, with pyridine-2-thiol and 2-benzoimidazol-2'-yl-pyridine as ligands, was prepared by Kim's group and used for CO_2 reduction with **EosinY**.[40] Sacrificial electron- and proton-donor was TEOA. The photocatalytic components were dissolved in a mixture of EtOH/H_2O (1:1) and irradiated at 420 nm for 10 hours. The only product observed was formate with a TON of 14000. This value was achieved at pH values of 10.7, and it gives the highest turnover frequency for HCO_2^- formation by a homogeneous noble-metal free catalytic system. Under an Ar-atmosphere, the same system produced molecular hydrogen (TON_{H2}: 1350, after 5 h), *via* a reversible protonated Ni-species. An oxidative quenching of **EosinY*** by **Ni2** is possible, as well as a reductive quenching by TEOA. However, the reductive quenching process is more plausible to occur, since TEOA is present in more considerable excess.

3. Earth-Abundant-Metal-Based Photosensitizers with Precious-Metal-Based Catalysts

Isolated examples of photoactivated CO_2-reduction by hybrid systems (noble-metal-free PS and noble-metal CAT) have been presented in the literature in the past five years. The work of Tsubomura group presented the development of various heteroleptic Cu(I)-based photosensitizers, which were employed in combination with the Re(I)-based carbonyl complex Re(bpy)$(CO)_3$Br, **Re1** (Figure 8).[41] The best results were achieved in a DMA/TEOA (4:1) solution, with 0.1 M BIH as electron donor and **Cu9** as PS. Although the emission quantum yield of Cu in this solvent mixture was lower than 0.01% and the lifetime was relatively short (30 ns), the reductive quenching by BIH was almost quantitative, according to Stern-Volmer data. Irradiation with a high-pressure Hg lamp at wavelengths higher than 370 nm for only 25 minutes gave CO as the sole product with a TON of 580 and a quantum efficiency of 37% (Table 3, entry 1).

Another example of a system using a Cu(I)-based PS and a Re(I)-based CAT was given by the work of Giereth *et al.*[42] **Cu1** was dissolved in a DMF/TEA (5% vol.) solution and, under white light irradiation, was reductively quenched by BIH. The reduced

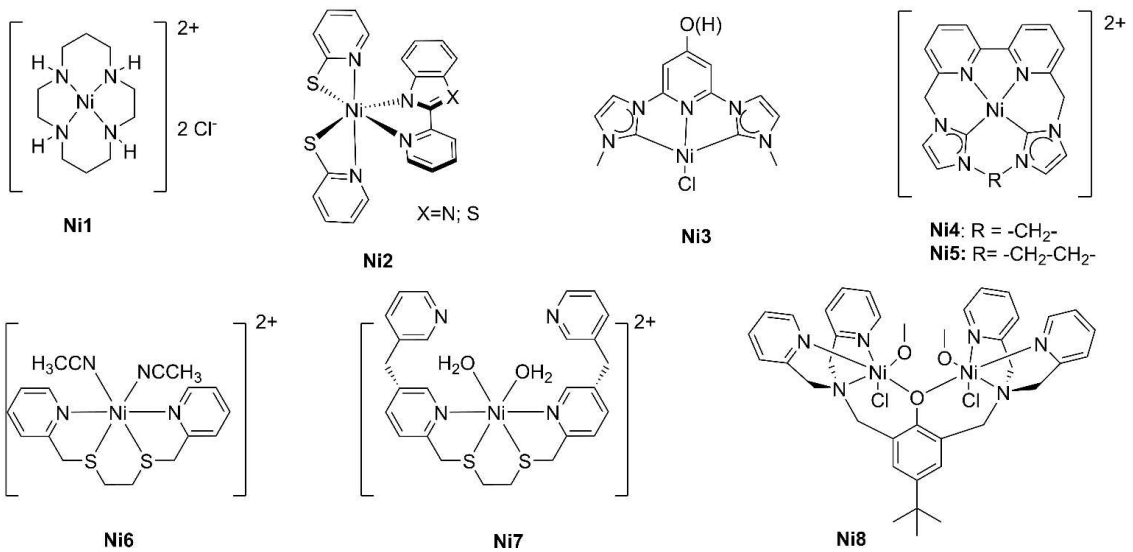

Figure 7. Ni(II)-based complexes presented in this review.

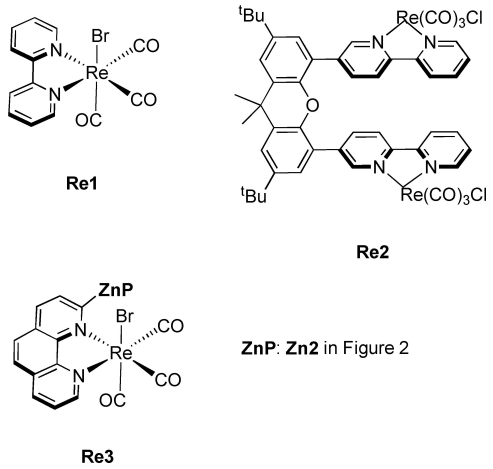

Figure 8. Chemical structures of the Re(I) carbonyl complexes that were used in combination with earth-abundant PS and discussed in this review.

Cu1$^-$ species can then reduce the binuclear complex **Re2** (see Figure 8) that reduces CO_2 to CO with a TON of 169, after 4 hours (Table 3, entry 2). A similar TON was determined when *fac*-Ir(dFppy)$_3$ was employed instead of **Cu1** (TON(Ir): 159). Nevertheless, this maximum TON was achieved already after 2 hours, implying a faster kinetic for the noble-metal system. Since **Re2** can also absorb light and work as a photocatalyst, it cannot be excluded that a part of the reduced **Re2** species was formed by direct reductive quenching of the catalyst excited-state by the sacrificial electron donor.

The last example of CO_2-reduction photoactivated by an earth-abundant Zn(II)-based porphyrin and a Re(I)-based catalyst was presented by Kuramochi *et al.*[43] In this case, the porphyrin and the Re catalyst are covalently bound at the *meso*-position of the macrocycle (**Re3**, Figure 8). The PS-CAT dyad was dissolved in DMA, containing BIH as e-D. The triplet excited state of the Zn(II)-moiety of **Zn2-Re3** was reductively quenched by the electron donor.

Interestingly, the phosphorescence of the zinc-porphyrin was observed in the dyad, thanks to the presence of the Re(I)-moiety, most probably because of the heavy-metal effect inducing strong spin-orbit coupling. The reduced Re(I)-moiety reduces CO_2 nearly quantitatively to carbon monoxide. The presence of the proton source phenol (0.1 M) in the homogeneous system enhanced the production of CO, reaching TON: 900 after 24 hours (Table 3, entry 3). The end of the catalysis was due to the consumption of BIH. In fact, adding further 500 equivalents of the e-D, the CO_2 reduction was reactivated and yielded a TON of 13000 after 60 hours in total.

4. Earth-Abundant-Metal-Based Catalysts with Precious Metal-Based Photosensitizers

More numerous works presented a hybrid system, bringing together a noble-metal-free catalyst and a precious metal-based photosensitizer. The reliability of the Ru(II)- and Ir(III)-based complexes is so strong that testing the efficiency of newly developed (earth-abundant) catalysts becomes vital with those PSs. The majority of works published in the last five years sees a cobalt-based catalyst with either **Ru(phen)$_3^{2+}$**, **Ru(bpy)$_3^{2+}$**, or **Ir(ppy)$_3$**, as the photosensitizer. Consistent contribution is given by the groups of Zhong and Lu, which elaborated several Co(II)-complexes based on cryptate ligands. In work published in 2017, a dinuclear Co complex (**Co15**, Figure 6) showed high efficiency and selectivity in the reduction of CO_2 to CO.[44] In particular, in an aqueous MeCN solution (25% H_2O), **Ru(phen)$_3^{2+}$** was employed as PS and TEOA as e-D. When the reaction was illuminated at 450 nm for 10 hours, the system produced CO with a TON of 16896 (Table 3, entry 4). Nevertheless, the quantum yield of the photocatalysis was only 0.04%. The peculiarity of the dinuclear complex **Co15**, as in other cryptates, is the optimal metal-metal separation, which enables synergistic catalysts. In **Co15**, one Co(II) core acts as the catalytic center while the other assists the catalysis by helping in the bond breakage between the C and O atom from the C(O)-OH intermediate. DFT theoretical calculations have also supported this. Moreover, it was observed that this complex could absorb CO_2 from the atmosphere to form a carbonate-bridged complex in a basic solution, which can undergo a proton-coupled electron transfer (PCET) by the PS.

However, it was impossible to distinguish which Co-atom was the catalytic site and which one was the assistant site. Thus, one year later, a Co(II)-Zn(II) cryptate binuclear complex (**Co16**, Figure 6) was prepared.[45] The Zn(II) role was to demonstrate the assistant site of the cryptate complex, as zinc has little activity towards CO_2 reduction, but a strong binding affinity with the hydroxy group. In similar photocatalytic conditions, **Co16** could obtain a TON of 65000 and a quantum yield of 0.15%. The corresponding mononuclear Co(II) derivative, **Co17**, showed a much lower efficiency (TON: 1500) and a selectivity of 74% (Table 3, entries 5 and 6). In the search of a strategy to improve the catalytic performance of tripodal cobalt complexes, the groups of Zhong and Lu investigated the effects of increasing the conjugation in the substituent, going from a phenyl (**Co18**), to a 1′-napthyl (**Co19**) and a 9′-anthracenyl (**Co20**).[46] The extended conjugation in **Co20** proved to be beneficial for the catalytic activity in regard to the reduction of CO_2 towards CO. In a photocatalytic system, consisting of **Ru(phen)$_3$** as photosensitizer and TEOA as e-Donor in CH3CN/H2O (4:1) solution, the catalysts **Co20** and **Co19** gave high TON numbers (12680 for **Co20** and 11280 for **Co19**) with selectivity up to 98% after 10 h irradiation at 450 nm (entries 7, 8 and 9, Table 3).The performance of **Co18** is one order of magnitude smaller, with a TON of 1600 and a lower selectivity (85%). When using a very small concentration of catalyst, 0.01 μmol, the TON values increased to 58000 (**Co20**) and 49200 (**Co19**). The effect of the conjugation was confirmed by electrochemistry, where the reduction of Co(II) to Co(I) is easier in **Co20** (−1.05 V vs NHE) than in **Co19** (−1.10 V vs NHE) and **Co18** (−1.20 V vs NHE), leading to much favourable thermodynamics for the oxidative quenching of **Ru(phen)$_3$***. The authors postulated that an additional effect is the formation of a π-π stacking

Table 3. Hybrid photocatalytic systems for CO_2 reduction using either noble-metal free PS or CAT.

Entry	PS	CAT	e-D	Solvent	λ_{exc}	Irradiation time	Products	TON	Selectivity [%]	Φ [%]	Ref.
1	**Cu9** (0.5 mM)	**Re1** (0.05 mM)	BIH (0.1 M)	DMA/TEOA	>370 nm	25 min	CO	580	>99	37	[41]
2	**Cu1** (50 μM)	**Re2** (50 μM)	BIH (10 mM)	DMF/TEA (5% v.)	>400 nm	4 h	CO	169	>99	–	[42]
3	**Zn2 – Re3** (0.05 M)		BIH (50 mM)	DMA + 0.1 M PhOH	420 nm	24 h	CO	>900	>99	8	[43]
4	**$Ru(phen)_3^{2+}$** (0.4 mM)	**Co15** (0.025 μM)	TEOA (0.3 M)	MeCN/H_2O (4/1)	450 nm	10 h	CO H_2	16896 (0.046 μmol)	98 2	0.04	[44]
5	**$Ru(phen)_3^{2+}$** (0.4 mM)	**Co16** (0.025 μM)	TEOA (0.3 M)	MeCN/H_2O (4/1)	450 nm	10 h	CO H_2	65000 (0.16 μmol)	98 2	0.15	[45]
6	**$Ru(phen)_3^{2+}$** (0.4 mM)	**Co17** (0.025 μM)	TEOA (0.3 M)	MeCN/H_2O (4/1)	450 nm	10 h	CO H_2	1500 (0.063 μmol)	74 26	–	[45]
7	**$Ru(phen)_3^{2+}$** (0.4 mM)	**Co18** (0.05 μM)	TEOA (0.3 M)	MeCN/H_2O (4/1)	450 nm	10 h	CO H_2	1600 (0.070 μmol)	85 15	0.04	[46]
8	**$Ru(phen)_3^{2+}$** (0.4 mM)	**Co19** (0.05 μM)	TEOA (0.3 M)	MeCN/H_2O (4/1)	450 nm	10 h	CO H_2	11280 (0.076 μmol)	97 3	0.17	[46]
9	**$Ru(phen)_3^{2+}$** (0.4 mM)	**Co20** (0.05 μM)	TEOA (0.3 M)	MeCN/H_2O (4/1)	450 nm	10 h	CO H_2	12680 (0.062 μmol)	98 2	0.19	[46]
10	**$Ru(phen)_3^{2+}$** (0.4 mM)	**Co20** (0.0125 μM)	TEOA (0.3 M)	MeCN/H_2O (4/1)	450 nm	10 h	CO H_2	51392 (0.032 μmol)	98 2	0.15	[47]
11	**$Ru(phen)_3^{2+}$** (0.4 mM)	**Co23** (0.025 μM)	TEOA (0.3 M)	MeCN/H_2O (4/1)	Blue LED, 15 W	3 h	CO H_2	14210 (0.10 μmol)	95 5	0.51	[48]
12	**$Ru(phen)_3^{2+}$** (0.4 mM)	**Co19** (0.05 μM)	TEA (0.3 M)	MeCN/H_2O (4/1)	450 nm	10 h	CO H_2	11600 (0.10 μmol)	97 3	0.27	[49]
13	**$Ru(phen)_3^{2+}$** (0.4 mM)	**Co7** (2 μM)	TEOA (0.3 M)	MeCN/H_2O (4/1)	450 nm	12 h	CO H_2	1330 (0.26 μmol)	98 2	0.27	[50]
14	**$Ir(ppy)_3$** (10 mM)	**Co8** (10 μM)	TEA	MeCN/TEA (4:1)	450 nm	60 h	CO H_2	91 23.2	80 20	–	[51]
15	**$Ru(phen)_3^{2+}$** (0.5 mM)	**Co9** (0.5 μM)	TEOA (0.3 M)	MeCN/H_2O (4:1)	>400 nm	10 h	CO H_2	2440 –	97 3	0.073	[52]
16	**$Ru(phen)_3^{2+}$** (0.5 mM)	**Co10** (0.25 μM)	TEOA (0.3 M)	MeCN/H_2O(4:1)	>400 nm	10 h	CO H_2	2600 (0.880 μmol)	97 3	–	[52]
17	**$Ir(ppy)_2$(qpy)-Co11** (0.1 mM)		BIH (80 mM)	MeCN + 2.5% TEA	450 nm	4 h	CO H_2	391 –	98 2	10.2 (1 h) 19.2 (425 nm)	[53]
18	**$Ru(phen)_3^{2+}$** (0.2 mM)	**Co12** (50 μM)	BIH (0.1 M)	MeCN + 20% TEOA	460 nm	60 h	HCO_2^- CO H_2	821 221 40	75.9 20.4 3.7	2.6 (12 h)	[54]
19	**$Ru(phen)_3^{2+}$** (0.2 mM)	**Co12** (50 μM)	BIH (0.1 M)	MeCN + PhOH (1 M)	460 nm	60 h	CO HCO_2^- H_2	829 12 22	96.0 1.4 2.6	–	[54]
20	**$Ru(phen)_3^{2+}$** (0.4 mM)	**Co13** (2.5 μM)	TEOA (0.4 M)	MeCN/H_2O (9:1)	469 nm	10 h	CO H_2	1450 (0.45 μmol)	95 5	–	[55]
21	**$Ru(bpy)_3^{2+}$** (0.5 mM)	**Co14** (0.15 μM)	TEOA (0.3 M)	MeCN/H_2O (4:1)	>400 nm	3 h	CO H_2	41017 (0.019 μmol)	87 13	0.94 (λ = 428 nm)	[56]
22	**$Ru(bpy)_3^{2+}$** (0.5 mM)	**Co5** (10 μM)	Ascorbate (0.1 M)	0.1 M $NaHCO_3$ buffer (pH 6.7)	>400 nm	4 h	CO H_2 HCO_2-	926 (19.7μmol) (6.6 μmol)	82	0.81 (λ = 428 nm)	[57]
23	**$Ru(phen)_3^{2+}$** (0.4 mM)	**Co24**	TEOA (0.3 M)	MeCN/H_2O (4:1)	450 nm	10 h	CO H_2	1302 (0.106 μmol)	98 2	0.26 (2 h)	[58]

Table 3. continued

Entry	PS	CAT	e-D	Solvent	λ_{exc}	Irradiation time	Products	TON	Selectivity [%]	Φ [%]	Ref.
24	**Ir(dFppy)$_3$** (50 μM)	**Co1** (50 μM)	TEA (5 %)	DMF	>400 nm	24 h	CO	90	>99	–	[36]
25	**Ir(ppy)$_3$** (0.2 mM)	**Fe1** (2 μM)	TEA (50 mM)	MeCN	>420 nm	47 h	CO H_2 CH_4	198 24 31	78 10 12	0.18 (for CH_4 after 102 h, in CO atm)	[59]
26	**Ir(ppy)$_3$** (0.2 mM)	**Fe9** (2 μM)	TEA (50 mM)	MeCN	>420 nm	47 h	CO H_2 CH_4	139 15 26	78 8 14	–	[59]
27	**Ru(phen)$_3^{2+}$** (0.2 mM)	**Fe10** (5 μM)	BIH (0.11 M)	MeCN/H_2O (1 : 1)	460 nm	68 h	CO H_2, HCO_2^-	14096 360 (traces)	98 2	0.8 (24 h)	[60]
28	**Ru(bpy)$_3^{2+}$** (0.5 mM)	**Fe11** (10 μM)	BIH (22 mM)	DMF/TEOA (7 : 1)	White light	6 h	CO H_2	19367 (1.29 μmol)	90 10	0.38 (5 h, 450 nm)	[61]
29	**Ir(ppy)$_3$** (0.1 mM)	**Ni3** (0.1 mM)	BIH (11 mM)	MeCN + 5 % TEA + 2 % H_2O	Solar simulator	6 h	CO	10.6	>99	–	[62]
30	**Ir(ppy)$_3$** (0.1 mM)	**Ni4** (2 nM)	BIH (10 mM)	MeCN + 5 % TEA + 2 % H_2O	Solar simulator	72 h	CO H_2 CH_4	8000 34000 5000	28 % (CO + CH_4) 72 %	–	[63a]
31	**Ir(ppy)$_3$** (0.1 mM)	**Ni5** (2 nM)	BIH (10 mM)	MeCN + 5 % TEA	Solar simulator	72 h	CO H_2 CH_4	175000 29000 19000	87 % (CO + CH_4) 13 %	–	[63a]
32	**Ru(bpy)$_3^{2+}$** (0.5 mM)	**Ni6** (30 μM)	BIH (0.1 M)	DMA/H_2O (9 : 1)	450 nm	55 h	CO	713	>99 %	1.42 %	[64]
33	**Ru(bpy)$_3^{2+}$** (0.5 mM)	**Ni7** (30 μM)	BIH (0.1 M)	DMA/H_2O (9 : 1) + Mg^{2+} (5 mM)	450 nm	1 h	CO	120	>99 %	11.1 %	[67]
34	**Ru(phen)$_3^{2+}$** (0.4 mM)	**Ni8** (5 μM)	TEOA (0.2 M)	MeCN/H_2O (4 : 1)	450 nm	12 h	CO	44	>99 %	0.2 %	[68]
35	**Ru(bpy)$_3^{2+}$** (2 mM)	**Cu13** (2.5 μM)	BIH (0.1 M)	MeCN + TEOA (15 %)	>420 nm	3.5 h	CO H_2	3730 490	88 % 12 %	–	[70]
36	**Ru(phen)$_3^{2+}$** (0.4 mM)	**Cu14** (0.5 μM)	TEOA (0.3 M)	MeCN/H2O (4 : 1)	450 nm	10 h	CO H_2	9900 200	98 % 2 %	–	[71]

interaction between the conjugated substituents with the photosensitizer, facilitating the photoinduced electron transfer.

Complex **Co22** is a mononuclear compound with a macrocyclic cryptand ligand with only one pocket occupied (Figure 6). Photocatalytic experiments were conducted in MeCN/H_2O (4:1) solution, with **Ru(phen)$_3^{2+}$** as the PS and BIH as e-D. After ten hours of irradiation at 450 nm, CO_2 was reduced to CO with 98% selectivity and a TON of 51392 (Table 3, entry 10). The calculated quantum yield was 0.15%, and the quenching mechanism of the PS was the oxidative process induced by the cobalt catalyst.[47]

The group of Martinho investigated the role of substituents on the aryl group of octaazacryptates. They synthesized a binuclear Co(II)-complexes, similar to those of Zhong and Lu, but with different substituents: –Br in **Co23**, –NO_2 in **Co24** and –CCH in **Co25** (Figure 6). Those complexes were employed in photoactivated CO_2-reduction in very similar conditions as the papers mentioned above. The best performing catalyst of this series was **Co25** with a TON of 14210 and a quantum efficiency of 0.51% after 3 hours (Table 3, entry11). This result was rationalized invoking the electron-donating nature of the alkynyl substituent, increasing the influence of the Co-cryptates on the capture of CO_2.[48] However, compound **Co23** produced methane after 30 hours of photocatalysis. Additional experiments proved that CO was an intermediate for the production of CH_4.

A mononuclear tripodal Co(II)-complex was formed by coordinating a cobalt ion with tris(2-(isopropylamino)ethylamine, **Co21**, which showed a catalytic activity toward photoactivated CO_2 reduction reaching TON_{CO} of 11600 and a selectivity of 98% after 10 hours of irradiation (Table 3, entry 12).[49] The authors compared the activity with the cobalt precursor $CoCl_2$, which, in the same conditions, gave a production of CO, although in a lower amount (TON: 4920). The photocatalytic system consisted of the same solvent mixture (MeCN/H_2O), like the previous works of Lu and Zhong groups, and **Ru(phen)$_3^{2+}$(PF$_6$)$_2$**, as PS. However, the electron donor was TEA instead of TEOA. The photocatalysis evolved carbon monoxide with a quantum efficiency of 0.27%, proceeding through an oxidative quenching of the Ru* by **Co21**.

The same authors reported another tripodal Co(II) complex with less basic functional groups: quinoline instead of isopropylamine (**Co7**, Figure 6). The CO_2 reduction was photoactivated by the same PS (**Ru(phen)$_3^{2+}$**) at 450 nm. The product was CO with 98% selectivity and a TON of 1330 (Table 3, entry 13). This value increases to TON 10650, when the concentration of the catalyst is reduced fifty times (0.04 μM).[50] Oxidative quenching of Ru* by **Co7**, produces a Co(I) species that binds CO_2 and continues the catalytic cycle. The presence of the quinolyl groups facilitates the cleavage of the C–O bond in the Co–C(O)OH intermediate due to an extended conjugation of the aromatic ring. The presence of water influences the catalytic activity and selectivity positively, inducing a lowering of the reduction potential of the Co–CO_2 adduct, due to a concerted PCET process.

Catalyst **Co8** was prepared by Zhu *et al.* and used in combination with **Ir(ppy)$_3$** as PS, in a solvent mixture of MeCN/TEA (4:1), where TEA is the e-D.[51] Also in this case, the photoactivation proceeds *via* an oxidative quenching of the PS* by the **Co8**, which reacts with CO_2 in its reduced state. The reaction underwent irradiation at 450 nm for 60 hours, and the turnover number of CO was 91.2 (Table 3, entry 14). Molecular hydrogen was produced simultaneously, lowering the selectivity towards C-product to 80%. Trace amounts of formic acid were also found. The addition of water led to an increase in H_2 production, which became the major product.

The mononuclear **Co9** and the dinuclear **Co10** complexes were investigated in the groups of Wei and Yuan.[52] Under visible-light irradiation (>400 nm) the **Ru(phen)$_3^{2+}$** PS was excited and underwent oxidative quenching by the Co(II)-catalyst. The electron donor TEOA repristinated the PS ground state. The gaseous products were analyzed, and after 10 hours, the TONs for carbon monoxide were 2440 and 2600 for **Co9** and **Co10**, respectively (Table 3, entries 15 and 16). This shows that the two catalysts have comparable activities. The slightly higher efficiency of the dinuclear complex **Co10** might indicate an independence of the two metal cores to bind and reduce CO_2.

Dynamic coordinative interaction between catalyst **Co11** and the PS based on Ir(III) complex raises the efficiency of the electron transfer process, enhancing the photoactivated CO_2-reduction, in the work of Ouyang and coworkers.[53] The PS is a **Ir(ppy)$_2$(qpy)** BF_4, where qpy is a 4,4′:2,2′,2″:4″,4′-quaterpyridine that coordinates axially the metal core of the **Co11** through the pendent pyridine. Within 4 hours, irradiation at 450 nm of the photocatalytic components, dissolved in a mixture of MeCN with 2.5% TEA and BIH as e-D, produced CO with a TON of 391 (Table 3, entry 17). Less than half of CO moles were produced by the system that contained **Ir(ppy)$_2$(bpy)** as a comparison PS. This indicates the enhanced efficiency of the electron transfer between the reduced **Ir(ppy)$_2$(qpy)**, formed by reductive quenching by BIH, and the metal core of the catalyst. Optimization of the quantum efficiency was done by changing the light source, reaching 19.2% when the system was irradiated at a 425 nm.

A binuclear pacman complex **Co12** can reduce CO_2 to formate or to carbon monoxide selectively, according to the reaction conditions. This selectivity control was achieved by the groups of Robert and Lau.[54] In particular, a selectivity of 75.9% towards HCO_2^- was obtained by irradiating a homogeneous solution in MeCN with 20% TEOA, where **Ru(phen)$_3^{2+}$**, **Co12** and BIH were employed as PS, CAT and e-D, respectively. The TON for formate after 60 hours of photocatalysis was 821, while TONco was 221 (Table 3, entry 18). The selectivity towards formate was enhanced to 91% when a heterogeneous semiconductor (**g-C3 N4**) was used as PS, while it dropped to 59% by using **Phen2** as PS. When 1 M phenol was used instead of TEOA, the same components started a photocatalysis that reached 96% selectivity towards CO (Table 3, entry 19). The catalytic process was investigated by electrochemistry. Under CO_2 atmosphere, catalytic potential was observed at −1.75 V (*versus* SCE), while it was positively shifted to −1.25 V in the presence of phenol, and to −1.5 V in the presence of TEA. It was therefore postulated that the binding of the CO_2 was done

in cooperativity by the two Co-cores and the different adduct depends on the conditions used. Thus, in the absence of a proton-donor like phenol, the two metal atoms bind CO_2 at the oxygen atoms (η^1_O for both atoms, see Figure 1), while in the presence of protons, one Co binds CO_2 at the carbon atom (η^1_C) and the other Co atom binds at the protonated oxygen (η^1_{OH}).

The photoactivated catalytic reduction of CO_2 to CO was obtained in an aqueous solution of MeCN and TEOA, by the phenanthroline based catalyst **Co13** together with the PS **Ru(phen)$_3^{2+}$**. Irradiation at 469 nm for 10 hours afforded the production of CO with a selectivity of 95% and a TON of 1450 (Table 3, entry 20).[55]

A pentacoordinating ligand was used by Chai *et al.* for the complexation of several first-row transition metals, and their catalytic activity towards CO_2 reduction was tested.[56] The cobalt-based complex **Co14** showed the best performance in terms of efficiency and selectivity. In a mixture of MeCN/H_2O (4:1), the photocatalysis was initiated by the excitation of **Ru(bpy)$_3^{2+}$** with visible light (>400 nm), which was oxidatively quenched by the CAT. The production of CO reached a turnover number of 41017 with a selectivity of 87% after 3 hours (see Table 3, entry 21). The quantum yield of the reaction was measured under irradiation at 428 nm, and it was 0.94%. However, it increased to 1.74% by increasing the concentration of **Co14** from 0.15 μM to 0.3 μM. When a Ni(II) core was used instead of cobalt, the TON was slightly lower (TON(Ni): 37854), while the analogous compounds made with Fe or Mn showed much lower efficiencies (TON(Fe): 18138; TON(Mn): 12350), although these data are also quite impressive.

Photocatalysis in water was achieved by the system published by Call *et al.* in 2019, using **Ru(byp)$_3^{2+}$** and **Co5** as PS and CAT, respectively.[57] The water solution was a $NaHCO_3$ buffer at pH 6.7, and sodium ascorbate was used as e-D. Photoirradiation under white light for 4 hours produced mainly CO with a TON of 926 (selectivity 82%). Molecular hydrogen was produced as a consequence of the reduction of water. The quantum yield was estimated after 1 hour of irradiation at 428 nm, and its value was 0.81% (Table 3, entry 22). Interesting kinetic studies performed by varying the catalyst concentration revealed an exponential increase of TON with decreasing [CAT], while the rate of the reaction decreases at higher [CAT]. On the other hand, the degradation of **Ru(byp)$_3^{2+}$** after 4 hours caused the suspension of the photocatalysis, which was reactivated by the addition of fresh PS.

In 2021, Liu *et al.* reported heterometallic binuclear complex of cobalt and zinc (**Co26**, Figure 6) and the analogous homometallic binuclear complex of cobalt (**Co27**), based on ligand 2,6-bis{[bis(2-pyridylmethyl)amino]methyl}-4-tert-butylphenol.[58] The **Co26** is another example of cooperative catalysis mediated by the two different metal centers, similar to the one obtained with complex **Co16** (see above), afforded by the favorable spatial distance between the two metal cores. Photochemical experiments were performed in MeCN/H_2O (4:1), containing **Ru(phen)$_3^{2+}$** as PS, TEOA as e-D, and the catalyst. Continuous irradiation at 450 nm for 10 hours produced CO in high selectivity (98%) and a TON of 1302 (Table 3, entry 23). The replacement of the zinc ion with a Co(II) decreased the efficiency, and the obtained TON was 890. However, when both cobalt ions were replaced with zinc, affording the correlative Zn(II)-Zn(II) complex, only traces of CO were formed. Stern-Volmer analyses demonstrated an oxidative quenching of Ru* by the catalyst **Co26** and the quantum efficiencies of the systems were estimated 0.26% and 0.17% for **Co26** and **Co27**, respectively. After 10 hours, the production of CO reached its plateau, caused by degradation of the PS. For a deep understanding of the improved activity of **Co26** in respect to **Co27**, theoretical calculations were carried out. The rate-limiting step was determined to be the CO_2 coordination, while the C–O bond cleavage requires a synergistic mechanism between the two metal cores. This step presents a lower energy barrier in the case of **Co26** over **Co27**, in accordance with the enhanced performance of **Co26**.

Rao *et al.* presented the iron porphyrins **Fe1** and **Fe9** to be able to reduce CO_2 to CO and subsequently to methane, in a photocatalytic system containing of **Ir(ppy)$_3$** as a photosensitizer,[59] one year before the noble-metal free system discussed above.[28] In particular, under white light irradiation in a CH_3CN solution with 50 mM TEA as e- donor, the photosensitizer is oxidatively quenched by **Fe1**. Further reduction processes generate the active Fe(0) state, which reduces CO_2. After 47 hours of irradiation, not only was CO found as a product (TON: 198), but also CH_4 (TON:31) and molecular hydrogen (TON: 24). Upon addition of trifluoroethanol, the yield of products increased, but the selectivity for CO decreased from 78% to 63%, while the selectivity of methane increased (from 12% to 17%). The production of CH_4 was demonstrated to happen in a second catalytic cycle by a Fe(II)-CO adduct, which after progressive reduction processes, leads to methane. Indeed, when the photocatalytic reaction was performed under a CO atmosphere, CH_4 evolved with a selectivity of 82%, besides H_2, and the quantum yield reached 0.18% (Table 3, entry 25). Catalyst **Fe9** could also produce methane with a TON of 26 after 47 h (Table 3, entry 26), while an unsubstituted Fe-tetraphenylporphyrin gave only CO and H_2 as products. This fact showed how the hydroxy groups in **Fe9** or the positively charged ammonium groups in **Fe1** are essential in stabilizing the Fe-CO adduct, which is the intermediate for the further reduction to CH_4.

An Fe(II)-based quinquepyridine complex (**Fe10**) was found to be highly efficient in photochemical CO_2-reduction by the groups of Robert and Lau.[60] Thanks to the increased chelating ability, the pentadentate ligand improved the stability of the iron complex compared to the corresponding tetradentate quaterpyridine. The photocatalysis was investigated in a H_2O/MeCN (1:1) solution. The PS, **Ru(phen)$_3^{2+}$**, was irradiated at 460 nm and was reductively quenched by BIH. The following electron transfer from the reduced Ru^- afforded the active species of **Fe10**, which can bind CO_2. Water acted as a base, and the replacement of TEOA with H_2O improved the catalytic activity (TON_{CO}:14095, after 68 h irradiation). The advantage of using water was also demonstrated by electrochemical experiments, where the addition of water resulted in a higher catalytic current under CO_2 atmosphere. Although the high amount of water present in the system, the selectivity towards CO was

excellent (98%); see Table 3, entry 27. The quantum yield of the photocatalysis was found to be 0.8% after 24 hours. A decreased water content (30%) gave 2.3% quantum efficiency.

The *ter*(phenanthroline)-Fe(II) complex (**Fe11**) was investigated for the CO_2 to CO reduction in a photocatalytic system that contained **Ru(byp)$_3$** as PS, BIH as e-D in a DMF/TEOA (7:1) solution.[61] The reductive quenching of the PS by BIH initiated the photocatalysis. After an induction period of ca. 20 minutes, the reduction of CO_2 started and decreased the rate almost after 80 minutes. However, the photocatalysis continued, and after 6 hours of irradiation under visible light, TON_{CO} reached the value of 19367. The selectivity was 90%, since also H_2 was observed (Table 3, entry 28). The photocatalytic quantum yield was determined to be 0.38% after 5 h at 450 nm.

A tetradentate pincer ligand, based on N-heterocyclic carbene (NHC) and pyridine, was used to coordinate Ni(II) ion to afford catalyst **Ni3**.[62] The presence of the hydroxyl group in *ortho* to the N-atom of the central pyridine can be either beneficial or adverse in CO_2 reduction. An *ad-hoc* study was performed by Papish and coworkers, who explored the efficiency of this catalyst in the protonated and de-protonated form. They prepared photocatalytic solutions in a solvent mixture of acetonitrile with 5% TEA, employing **Ir(ppy)$_3$** as PS. Under illumination from a solar simulator for 6 hours, the deprotonated form of **Ni3** produced carbon monoxide with a TON of 10.6 (Table 3, entry 29). An analogous Ni(II) complex, without the hydroxy group, in the same conditions, gave only 0.09. The protonated form of **Ni3** was achieved by adding triflic acid to the photocatalytic system, which then yielded a TON_{CO} of 0.9. The dramatic efficiency decrease might be related to the lower electron-donating ability of OH compared to O^-, yielding a diminished electron density to the metal center.

Jurss and Delcamp developed bipyridyl-N-heterocyclic-carbene macrocyclic Ni(II) complexes (**Ni4** and **Ni5**), providing a robust metal-ligand bonding interaction, supported by the strong sigma-donor ability of the NHC.[63] Using **Ir(ppy)$_3$** as PS and BIH as e-D, a reductive quenching process occurs under the irradiation of a solar simulator. In the absence of BIH, oxidative quenching pathways by the Ni(II)-based catalyst becomes possible. These catalysts are very efficient in photoactivated CO_2-reduction. In the absence of water, the generated CO reached TON values of 76000 and 310000 for **Ni4** and **Ni5**, respectively, with selectivity up to 90%. When 2% of water was added, the selectivity got lower, as H_2 production increased. Nevertheless, CH_4 was observed. In particular, the $TON_{(CH4)}$ for the two catalytic systems was 5000 (**Ni4**) and 19000 (**Ni5**) after 72 hours of irradiation (Table 3, entries 30 and 31). Kinetic studies showed that the evolution of CH_4 started after 4 hours; in parallel CO and H_2 concentrations decreased. The authors supposed that the same catalyst also acted as a hydrogenation catalyst for carbon monoxide. Thus, when performing photocatalytic experiments under an atmosphere of CO:H_2 (1:1), methane was the only product with a TON of 570000 (after 72 h under white light).

A bioinspired Ni(II) complex, **Ni6**, with the S_2N_2 tetradentate ligand bis(2-pyridylmethyl)-1,2-ethanedithiol, was explored in Kojima's group.[64] The presence of the sulfur atoms in the ligands can stabilize Ni(I) and Ni(0) species, which are intermediated in the catalytic cycle. In DMA/H_2O (9:1), the photocatalysis occurred *via* reductive quenching of **Ru(bpy)$_3^{2+}$** by BIH, followed by reduction of **Ni6**, which is able – in its low-valent state- to make an adduct with CO_2 and reduce it. After 55 hours of irradiation at 450 nm, the TON_{CO} was 713 (Table 3, entry 32). The quantum efficiency was found to be 1.42%. Interestingly, the same catalyst is also active towards the electro- and photocatalytic H_2 evolution.[65] Computational studies on the photocatalytic CO_2 reduction by **Ni6** were performed by Zhang *et al.*[66]

The catalytic performance of **Ni6** was improved by a slightly different ligand design, which consisted of additional pyridine rings that form a chelating pocket, able to accommodate a Lewis acidic metal ion, such as Mg^{2+} (see **Ni7** in Figure 7).[67] The role of Mg^{2+} is to stabilize the CO_2-Ni(0) adduct. Nevertheless, the electrochemical properties of **Ni7** remain very similar to those of **Ni6**. Photocatalysis was performed under the same conditions employed in the work for **Ni6**, and already after one hour, the selective production of CO yielded a TON of 120 and a quantum efficiency of 11.1% (Table 3, entry 33). The evolution of CO is faster in the presence of Mg^{2+} also when **Ni6** was used. Other metal ions, like Ca^{2+} and Zn^{2+}, showed likewise an increase in the photocatalysis, comparable to those obtained with Mg^{2+}.

In catalyst **Ni8**, developed by Wang *et al.*, two Ni(II) centers are coordinated by 2,6-bis((bis(pyridin-2-ylmethyl)amino)-methyl)-4-(tert-butyl)phenol ligand.[68] The Ni–Ni distance of 3.950 Å is advantageous for the cooperative activation of CO_2. The photocatalytic experiments were conducted in MeCN/H_2O (4:1) under irradiation at 450 nm. **Ru(phen)$_3^{2+}$** was chosen as PS and TEOA (0.2 M) as e-D. CO was the only product observed, besides some traces of H_2, and the photocatalytic system afforded a TON of 44 after 12 h, with a quantum yield of 0.2% (Table 3, entry 34).

However, the catalysis reached a plateau after 8 hours already, most probably because of the decomposition of **Ru(phen)$_3^{2+}$**.

Very few examples reported Cu(II)-based catalysts for CO_2 reduction in these past years. A first example is given by the quaterpyridine (qpy) complex **Cu13** shown in Figure 9.

Previously, quaterpyridine complexes of iron and cobalt were successfully exploited in the CO_2 reduction, and nowadays are still in the spotlight as electrocatalysts, or in combination with heterogeneous photosensitizers.[69] The work of Guo *et al.* showed that also Cu(qpy) complexes can effectively reduce CO_2

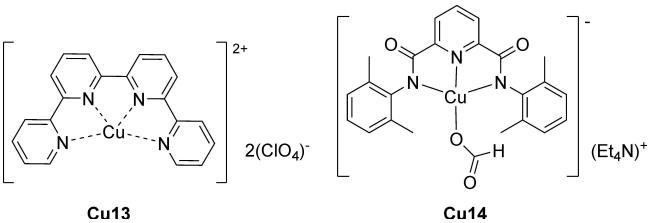

Figure 9. Cu(II)-based catalysts presented in this review.

to CO with high selectivity.[70] In a CH_3CN solution with 15% of TEOA, **Ru(bpy)$_3^{2+}$** was reductively quenched by BIH under irradiation of visible light ($\lambda \geq 420$ nm). After 3.5 hours, **Cu13** generated CO with a TON of 3730 and H_2 (TON: 490). Interestingly, when using a higher amount of catalyst (5 μM instead of 2.5 μM), also formic acid could be detected (TON:8). Very high TON (12400) for CO production was obtained when 1 μM **Cu13** was used in the presence of 3% H_20. Although the evolvement of H_2 increased as well, the selectivity of CO reached 97% (entry 35, Table 3). Interestingly, as the reduction of Cu(II) in **Cu13** occurs already at 0.1 V (*vs.* SCE) dimerizing, BIH can reduce **Cu13** already before irradiation, forming a $Cu_2(qpy)_2$ species, which was confirmed by electrospray ionization mass spectroscopy (ESI-MS). This dimer is then further reduced to Cu(0) or Cu(I)$(qpy)^-$ by **Ru(bpy)$_3^{+}$**. Experiments in the presence of Hg gave a 10% decrease in CO evolvement, indicating that a small amount of Cu(0) nanoparticles could form and be involved in the catalysis. However, the catalysis is predominantly homogeneous.

The second example of a Cu(II)-based catalyst is given by the complex formed by coordinating the *N,N,N*-pincer ligand, bis(2,6-dimethylphenyl)-2,6-pyridinedicarboxamidate, with a Cu(II) ion.[71] The metal ion is further coordinated by a formate anion so that the total charge of the complex **Cu14** is negative (Figure 9). This complex can oxidatively quench the excited state of **Ru(phen)$_3^{2+}$** in a solution of CH_3CN/H_2O (4:1), irradiated at 450 nm. After 10 hours of photocatalysis, **Cu14** produced CO with a TON of 9900 and a selectivity of 98% towards molecular hydrogen. (Table 3, entry 36). The production of CO was stopped after 10 hours because of the degradation of the photosensitizer. Thus, the activity was repristinated upon the addition of fresh **Ru(phen)$_3^{2+}$**. DFT calculations helped in evaluating the catalytic mechanism. At a redox potential of −0.95 V (*vs.* NHE), the complex is reduced to Cu(I) and forms an adduct with CO_2 (of type η^1_C, Figure 3). Molecular orbital analyses gave further insight, showing that in the transition state, a square-planar conformation of a d^8 Cu(III) species is built, after 2 electrons donation to the CO_2. The following PCET occurs with the subsequent cleavage of a C–OH bond, yielding to CO.

5. Conclusions and Perspectives

Research on developing environmentally-friendly and noble-metal-free photosensitizers and catalysts for CO_2-reduction is desirable. The development of fully earth-abundant-metal systems is still a minority in photoactivated CO_2-reduction, as the main focus is on the search for new efficient catalysts rather than the optimization of the whole photocatalytic process. This is reflected by the fact that the attention is to optimize the reactions so that the turnover numbers increase as an indication of the catalyst efficiency, but the quantum yield of the photoreaction is most of the time overlooked and sometimes even absent. Another important aspect, which is often neglected, is the evaluation of the redox properties of the excited state of the photosensitizers in the solvent mixture, where photocatalysis occurs. Frequently, those values are taken from reported literature, and the solvent effects are not considered. Generally, remarkable steps forward have been taken over the past years regarding photoactivated CO_2-reduction. In addition, looking for more sustainable pathways, researchers should find an alternative to the use of a sacrificial electron donor. A possible way to overcome this problem is by photoelectrochemical cells, where the advantages of photocatalysis and electrocatalysis are combined.[22d,72]

Nevertheless, several challenges still remain to be achieved. One of these future tasks is to go beyond the two-electrons reduction and achieve methanol, methane, and multi-carbon products, maybe exploiting cooperativity between two or more metals. Most of the time, photocatalytic experiments employ organic solvents, which are not environmentally friendly. Thus, the optimization of such reactions should consider utilizing more sustainable alternatives. The same can be said for the use of sacrificial electron donors. In fact, its use avoids upstream that the entire process is sustainable. Last but not least, it is essential to develop new noble-metal-free photosensitizers and catalysts that are highly photostable. Much has been done and even more is head-of us to close the carbon cycle, exploit the most abundant energy source (sunlight), and achieve a sustainable society.

Acknowledgements

The author thanks financial support from the German Research Society (DFG) through the Collaborative Research Center SFB/TRR88 "Cooperative Effects in Homo and Heterometallic Complexes (3MET)", support from the Young Investigator Network of the Karlsruhe Institute of Technology (KIT) and the state of Baden-Wuerttemberg. Furthermore, the entire "Bizzarri Team" is acknowledged for being such a good research team, keeping high motivation through the challenges of chemistry and beyond. Open Access funding enabled and organized by Projekt DEAL.

Conflict of Interest

There are no conflicts to declare.

Keywords: Artificial Photosynthesis · Carbon Dioxide Reduction · Earth-Abundant Metal Complexes · Noble-Metal-Free · Photocatalysis

[1] U. Nation in *COP26 closes with 'compromise' deal on climate, but it's not enough, says UN chief*, *Vol.* **2021**, p. https://news.un.org/en/story/2021/2011/1105792.
[2] a) S. Dabral, T. Schaub, *Adv. Synth. Catal.* **2019**, *361*, 223–246; b) Q. Liu, L. Wu, R. Jackstell, M. Beller, *Nat. Commun.* **2015**, *6*, 5933; c) J. Artz, T. E. Müller, K. Thenert, J. Kleinekorte, R. Meys, A. Sternberg, A. Bardow, W. Leitner, *Chem. Rev.* **2018**, *118*, 434–504.
[3] Y. Yamazaki, H. Takeda, O. Ishitani, *J. Photochem. Photobiol. C* **2015**, *25*, 106–137.
[4] Y. Pellegrin, F. Odobel, *C R Chimie* **2017**, *20*, 283–295.

[5] R. N. Sampaio, D. C. Grills, D. E. Polyansky, D. J. Szalda, E. Fujita, *J. Am. Chem. Soc.* **2020**, *142*, 2413–2428.
[6] a) Y. Zhang, M. Schulz, M. Wächtler, M. Karnahl, B. Dietzek, *Coord. Chem. Rev.* **2018**, *356*, 127–146; b) P. A. Forero Cortés, M. Marx, M. Trose, M. Beller, *Chem Catalysis* **2021**, *1*, 298–338.
[7] S. Garakyaraghi, E. O. Danilov, C. E. McCusker, F. N. Castellano, *J. Phys. Chem. A* **2015**, *119*, 3181–3193.
[8] a) N. A. Romero, D. A. Nicewicz, *Chem. Rev.* **2016**, *116*, 10075–10166; b) Y. Wu, D. Kim, T. S. Teets, *Synlett*; c) L. Marzo, S. K. Pagire, O. Reiser, B. König, *Angew. Chem. Int. Ed.* **2018**, *57*, 10034–10072; *Angew. Chem.* **2018**, *130*, 10188–10228.
[9] C.-F. Leung, T.-C. Lau, *Energy Fuels* **2021**.
[10] R. C. Society in *https://www.rsc.org/periodic-table/element/26/iron*, *Vol*.
[11] R. C. Society in *https://www.rsc.org/periodic-table/element/25/manganese*, *Vol*.
[12] R. C. Society in *https://www.rsc.org/periodic-table/element/27/cobalt*, *Vol*.
[13] S. van den Brink, R. Kleijn, B. Sprecher, A. Tukker, *Resour. Conserv. Recycl.* **2020**, *156*, 104743.
[14] a) F. Wang, *ChemSusChem* **2017**, *10*, 4393–4402; b) C. Li, X. Tong, P. Yu, W. Du, J. Wu, H. Rao, Z. M. Wang, *J. Mater. Chem. A* **2019**, *7*, 16622–16642.
[15] R. C. Society in *https://www.rsc.org/periodic-table/element/28/nickel*, *Vol*.
[16] H. Dobbek, V. Svetlitchnyi, L. Gremer, R. Huber, O. Meyer, *Science* **2001**, *293*, 1281–1285.
[17] M. Beley, J.-P. Collin, R. Ruppert, J.-P. Sauvage, *J. Chem. Soc. Chem. Commun.* **1984**, 1315–1316.
[18] V. S. Thoi, N. Kornienko, C. G. Margarit, P. Yang, C. J. Chang, *J. Am. Chem. Soc.* **2013**, *135*, 14413–14424.
[19] T. Kojima, *ChemPhotoChem* **2021**, *5*, 512–520.
[20] L.-M. Cao, H.-H. Huang, J.-W. Wang, D.-C. Zhong, T.-B. Lu, *Green Chem.* **2018**, *20*, 798–803.
[21] a) D. Walther, M. Ruben, S. Rau, *Coord. Chem. Rev.* **1999**, *182*, 67–100; b) M. Cokoja, C. Bruckmeier, B. Rieger, W. A. Herrmann, F. E. Kühn, *Angew. Chem. Int. Ed.* **2011**, *50*, 8510–8537; *Angew. Chem.* **2011**, *123*, 8662–8690; c) S. Straub, P. Vöhringer, *Angew. Chem. Int. Ed.* **2021**, *60*, 2519–2525; *Angew. Chem.* **2021**, *133*, 2549–2555.
[22] a) H. Takeda, C. Cometto, O. Ishitani, M. Robert, *ACS Catal.* **2017**, *7*, 70–88; b) A. Rosas-Hernández, C. Steinlechner, H. Junge, M. Beller, *Top. Curr. Chem.* **2017**, *376*, 1; c) Y. Zhao, Z. Liu, *Chin. J. Chem.* **2018**, *36*, 455–460; d) K. E. Dalle, J. Warnan, J. J. Leung, B. Reuillard, I. S. Karmel, E. Reisner, *Chem. Rev.* **2019**, *119*, 2752–2875; e) E. Boutin, L. Merakeb, B. Ma, B. Boudy, M. Wang, J. Bonin, E. Anxolabéhère-Mallart, M. Robert, *Chem. Soc. Rev.* **2020**, *49*, 5772–5809; f) H. Chen, L. Chen, G. Chen, M. Robert, T.-C. Lau, *ChemPhysChem* **2021**, *22*, 1835–1843; g) X. Guan, S. S. Mao, S. Shen, *ChemNanoMat* **2021**, *7*, 873–880; h) N. Elgrishi, M. B. Chambers, X. Wang, M. Fontecave, *Chem. Soc. Rev.* **2017**, *46*, 761–796; i) M. Đokić, H. S. Soo, *Chem. Commun.* **2018**, *54*, 6554–6572; j) D.-C. Liu, D.-C. Zhong, T.-B. Lu, *EnergyChem* **2020**, *2*, 100034.
[23] H. Takeda, H. Kamiyama, K. Okamoto, M. Irimajiri, T. Mizutani, K. Koike, A. Sekine, O. Ishitani, *J. Am. Chem. Soc.* **2018**, *140*, 17241–17254.
[24] a) C. Steinlechner, A. F. Roesel, E. Oberem, A. Päpcke, N. Rockstroh, F. Gloaguen, S. Lochbrunner, R. Ludwig, A. Spannenberg, H. Junge, R. Francke, M. Beller, *ACS Catal.* **2019**, *9*, 2091–2100; b) C. Steinlechner, A. F. Roesel, E. Oberem, A. Päpcke, N. Rockstroh, F. Gloaguen, S. Lochbrunner, R. Ludwig, A. Spannenberg, H. Junge, R. Francke, M. Beller, *ACS Catal.* **2020**, *10*, 578–579.
[25] J. D. Shipp, H. Carson, S. J. P. Spall, S. C. Parker, D. Chekulaev, N. Jones, M. Y. Mel'nikov, C. C. Robertson, A. J. H. M. Meijer, J. A. Weinstein, *Dalton Trans.* **2020**, *49*, 4230–4243.
[26] H. Koizumi, H. Chiba, A. Sugihara, M. Iwamura, K. Nozaki, O. Ishitani, *Chem. Sci.* **2019**, *10*, 3080–3088.
[27] H. Rao, J. Bonin, M. Robert, *ChemSusChem* **2017**, *10*, 4447–4450.
[28] H. Rao, C.-H. Lim, J. Bonin, G. M. Miyake, M. Robert, *J. Am. Chem. Soc.* **2018**, *140*, 17830–17834.
[29] a) A. Rosas-Hernández, C. Steinlechner, H. Junge, M. Beller, *Green Chem.* **2017**, *19*, 2356–2360; b) P. A. Forero-Cortés, M. Marx, N. G. Moustakas, F. Brunner, C. E. Housecroft, E. C. Constable, H. Junge, M. Beller, J. Strunk, *Green Chem.* **2020**, *22*, 4541–4549.
[30] Y. Sakaguchi, A. Call, M. Cibian, K. Yamauchi, K. Sakai, *Chem. Commun.* **2019**, *55*, 8552–8555.
[31] L. Chen, Y. Qin, G. Chen, M. Li, L. Cai, Y. Qiu, H. Fan, M. Robert, T.-C. Lau, *Dalton Trans.* **2019**, *48*, 9596–9602.
[32] a) Y. Wang, X.-W. Gao, J. Li, D. Chao, *Chem. Commun.* **2020**, *56*, 12170–12173; b) Y. Wang, T. Liu, L. Chen, D. Chao, *Inorg. Chem.* **2021**, *60*, 5590–5597; c) Y. Wang, L. Chen, T. Liu, D. Chao, *Dalton Trans.* **2021**, *50*, 6273–6280.
[33] H. Takeda, Y. Monma, O. Ishitani, *ACS Catal.* **2021**, *11*, 11973–11984.
[34] H. Takeda, K. Ohashi, A. Sekine, O. Ishitani, *J. Am. Chem. Soc.* **2016**, *138*, 4354–4357.
[35] H. Yuan, B. Cheng, J. Lei, L. Jiang, Z. Han, *Nat. Commun.* **2021**, *12*, 1835.
[36] M. Obermeier, F. Beckmann, R. S. Schaer, O. S. Wenger, M. Schwalbe, *Front. Chem.* **2021**, *9*.
[37] X. Zhang, M. Cibian, A. Call, K. Yamauchi, K. Sakai, *ACS Catal.* **2019**, *9*, 11263–11273.
[38] X. Zhang, K. Yamauchi, K. Sakai, *ACS Catal.* **2021**, *11*, 10436–10449.
[39] L.-L. Gracia, L. Luci, C. Bruschi, L. Sambri, P. Weis, O. Fuhr, C. Bizzarri, *Chem. Eur. J.* **2020**, *26*, 9929–9937.
[40] S. E. Lee, A. Nasirian, Y. E. Kim, P. T. Fard, Y. Kim, B. Jeong, S.-J. Kim, J.-O. Baeg, J. Kim, *J. Am. Chem. Soc.* **2020**, *142*, 19142–19149.
[41] Y. Yamazaki, T. Onoda, J. Ishikawa, S. Furukawa, C. Tanaka, T. Utsugi, T. Tsubomura, *Front. Chem.* **2019**, *7*, 288.ACS Appl. Energ. Mater.
[42] R. Giereth, M. Obermeier, L. Forschner, M. Karnahl, M. Schwalbe, S. Tschierlei, *ChemPhotoChem* **2021**, *5*, 644–653.
[43] Y. Kuramochi, Y. Fujisawa, A. Satake, *J. Am. Chem. Soc.* **2020**, *142*, 705–709.
[44] T. Ouyang, H.-H. Huang, J.-W. Wang, D.-C. Zhong, T.-B. Lu, *Angew. Chem. Int. Ed.* **2017**, *56*, 738–743; *Angew. Chem.* **2017**, *129*, 756–761.
[45] T. Ouyang, H.-J. Wang, H.-H. Huang, J.-W. Wang, S. Guo, W.-J. Liu, D.-C. Zhong, T.-B. Lu, *Angew. Chem. Int. Ed.* **2018**, *57*, 16480–16485; *Angew. Chem.* **2018**, *130*, 16718–16723.
[46] D.-C. Liu, H.-J. Wang, T. Ouyang, J.-W. Wang, L. Jiang, D.-C. Zhong, T.-B. Lu, *ACS Appl. Energ. Mater.ater.* **2018**, *1*, 2452–2459.
[47] D.-C. Liu, H.-J. Wang, J.-W. Wang, D.-C. Zhong, L. Jiang, T.-B. Lu, *Chem. Commun.* **2018**, *54*, 11308–11311.
[48] S. Realista, J. C. Almeida, S. A. Milheiro, N. A. G. Bandeira, L. G. Alves, F. Madeira, M. J. Calhorda, P. N. Martinho, *Chem. Eur. J.* **2019**, *25*, 11670–11679.
[49] D.-C. Liu, H.-H. Huang, J.-W. Wang, L. Jiang, D.-C. Zhong, T.-B. Lu, *ChemCatChem* **2018**, *10*, 3435–3440.
[50] J.-W. Wang, H.-H. Huang, J.-K. Sun, T. Ouyang, D.-C. Zhong, T.-B. Lu, *ChemSusChem* **2018**, *11*, 1025–1031.
[51] C.-Y. Zhu, Y.-Q. Zhang, R.-Z. Liao, W. Xia, J.-C. Hu, J. Wu, H. Liu, F. Wang, *Dalton Trans.* **2018**, *47*, 13142–13150.
[52] L. Zhang, S. Li, H. Liu, Y.-S. Cheng, X.-W. Wei, X. Chai, G. Yuan, *Inorg. Chem.* **2020**, *59*, 17464–17472.
[53] J.-W. Wang, L. Jiang, H.-H. Huang, Z. Han, G. Ouyang, *Nat. Commun.* **2021**, *12*, 4276.
[54] Z. Guo, G. Chen, C. Cometto, B. Ma, H. Zhao, T. Groizard, L. Chen, H. Fan, W.-L. Man, S.-M. Yiu, K.-C. Lau, T.-C. Lau, M. Robert, *Nature Catalysis* **2019**, *2*, 801–808.
[55] C.-L. Wang, J. Du, H. Yang, S.-Z. Zhan, *Catal. Lett.* **2021**.
[56] X. Chai, H.-H. Huang, H. Liu, Z. Ke, W.-W. Yong, M.-T. Zhang, Y.-S. Cheng, X.-W. Wei, L. Zhang, G. Yuan, *Chem. Commun.* **2020**, *56*, 3851–3854.
[57] A. Call, M. Cibian, K. Yamamoto, T. Nakazono, K. Yamauchi, K. Sakai, *ACS Catal.* **2019**, *9*, 4867–4874.
[58] D. Liu, M. Zhang, H.-H. Huang, Q. Feng, C. Su, A. Mo, J.-W. Wang, Z. Qi, X. Zhang, L. Jiang, Z. Chen, *ACS Sustainable Chem. Eng.* **2021**, *9*, 9273–9281.
[59] H. Rao, L. C. Schmidt, J. Bonin, M. Robert, *Nature* **2017**, *548*, 74–77.
[60] Y. Qin, L. Chen, G. Chen, Z. Guo, L. Wang, H. Fan, M. Robert, T.-C. Lau, *Chem. Commun.* **2020**, *56*, 6249–6252.
[61] Z.-C. Fu, C. Mi, Y. Sun, Z. Yang, Q.-Q. Xu, W.-F. Fu, *Molecules* **2019**, *24*, 1878.
[62] D. B. Burks, S. Davis, R. W. Lamb, X. Liu, R. R. Rodrigues, N. P. Liyanage, Y. Sun, C. E. Webster, J. H. Delcamp, E. T. Papish, *Chem. Commun.* **2018**, *54*, 3819–3822.
[63] a) H. Shirley, X. Su, H. Sanjanwala, K. Talukdar, J. W. Jurss, J. H. Delcamp, *J. Am. Chem. Soc.* **2019**, *141*, 6617–6622; b) X. Su, K. M. McCardle, J. A. Panetier, J. W. Jurss, *Chem. Commun.* **2018**, *54*, 3351–3354.
[64] D. Hong, Y. Tsukakoshi, H. Kotani, T. Ishizuka, T. Kojima, *J. Am. Chem. Soc.* **2017**, *139*, 6538–6541.
[65] D. Hong, Y. Tsukakoshi, H. Kotani, T. Ishizuka, K. Ohkubo, Y. Shiota, K. Yoshizawa, S. Fukuzumi, T. Kojima, *Inorg. Chem.* **2018**, *57*, 7180–7190.
[66] B. Zhang, S. Yang, X. Zheng, Y.-w. Ju, B.-Z. Chen, *Organometallics* **2020**, *39*, 1176–1186.
[67] D. Hong, T. Kawanishi, Y. Tsukakoshi, H. Kotani, T. Ishizuka, T. Kojima, *J. Am. Chem. Soc.* **2019**, *141*, 20309–20317.
[68] J.-W. Wang, J.-K. Sun, D.-C. Liu, L. Jiang, *Eur. J. Inorg. Chem.* **2020**, *2020*, 4450–4453.

[69] a) C. Cometto, L. Chen, D. Mendoza, B. Lassalle-Kaiser, T.-C. Lau, M. Robert, *ChemSusChem* **2019**, *12*, 4500–4505; b) C. Cometto, R. Kuriki, L. Chen, K. Maeda, T.-C. Lau, O. Ishitani, M. Robert, *J. Am. Chem. Soc.* **2018**, *140*, 7437–7440; c) Z. Guo, S. Cheng, C. Cometto, E. Anxolabéhère-Mallart, S.-M. Ng, C.-C. Ko, G. Liu, L. Chen, M. Robert, T.-C. Lau, *J. Am. Chem. Soc.* **2016**, *138*, 9413–9416; d) M. Loipersberger, D. G. A. Cabral, D. B. K. Chu, M. Head-Gordon, *J. Am. Chem. Soc.* **2021**, *143*, 744–763.
[70] Z. Guo, F. Yu, Y. Yang, C.-F. Leung, S.-M. Ng, C.-C. Ko, C. Cometto, T.-C. Lau, M. Robert, *ChemSusChem* **2017**, *10*, 4009–4013.
[71] W.-J. Liu, H.-H. Huang, T. Ouyang, L. Jiang, D.-C. Zhong, W. Zhang, T.-B. Lu, *Chem. Eur. J.* **2018**, *24*, 4503–4508.
[72] a) Y. Wang, D. He, H. Chen, D. Wang, *J. Photochem. Photobiol. C* **2019**, *40*, 117–149; b) N. Nandal, S. L. Jain, *Coord. Chem. Rev.* **2022**, *451*, 214271.
[73] E. Mejía, S.-P. Luo, M. Karnahl, A. Friedrich, S. Tschierlei, A.-E. Surkus, H. Junge, S. Gladiali, S. Lochbrunner, M. Beller, *Chem. Eur. J.* **2013**, *19*, 15972–15978.
[74] N. Armaroli, F. Diederich, L. Echegoyen, T. Habicher, L. Flamigni, G. Marconi, J.-F. Nierengarten, *New J. Chem.* **1999**, *23*, 77–83.
[75] C. Grazia, C. Clementi, C. Miliani, A. Romani, *Photochem. Photobiol. Sci.* **2011**, *10*, 1249–1254.
[76] F. Monti, A. Baschieri, L. Sambri, N. Armaroli, *Acc. Chem. Rev.* **2021**, *54*, 1492–1505.
[77] Y. Du, R. M. Pearson, C.-H. Lim, S. M. Sartor, M. D. Ryan, H. Yang, N. H. Damrauer, G. M. Miyake, *Chem. Eur. J.* **2017**, *23*, 10962–10968.
[78] C. K. Prier, D. A. Rankic, D. W. C. MacMillan, *Chem. Rev.* **2013**, *113*, 5322–5363.
[79] K. Teegardin, J. I. Day, J. Chan, J. Weaver, *Org. Process Res. Dev.* **2016**, *20*, 1156–1163.

Manuscript received: February 17, 2022
Revised manuscript received: April 5, 2022
Accepted manuscript online: April 9, 2022